Electron-phonon coupling and surface-state polarons on Si(111)2×1

C. D. Chen
International School for Advanced Studies, Trieste, Italy

A. Selloni
Istituto di Fisica "G. Marconi," University of Rome, Italy

E. Tosatti
International School for Advanced Studies, Trieste, Italy; Gruppo Nazionale di Struttura della Materia; Unità di Trieste, Italy; and International Centre for Theoretical Physics, Trieste, Italy

(Received 9 April 1984)

Electrons in surface states are usually treated decoupled from lattice motion. In reality, that coupling is at least as important as in the bulk, and possibly much more so, for surface bands are generally narrower. We present here a theory of polaron effects on the dangling-bond states of the Si(111)2×1 reconstructed surface, probably the best-studied crystal surface in every other respect. In view of the current debate over the nature of the reconstruction, we consider two alternative situations, ionic buckling (Haneman model) and covalent π-bonded chains (Pandey model). With parameters chosen to approximate as closely as possible the known experimental facts, the buckled surface is found to be strong coupling with small surface-state polarons, while the π-bonded surface is a relatively weak-coupling case. Among other things, the temperature-dependent red shifts of optical-absorption lines predicted for the two situations are different by almost 1 order of magnitude. This study provides a first theoretical illustration of large- and small-polaron effects on surface states. It could also specifically help discriminating between 2×1 reconstruction models of the Si(111) surface, when its temperature-dependent spectroscopy becomes available. We finally discuss the general relevance of polaron effects in experimental surface-state spectroscopic studies, including optical absorption and luminescence, as well as photoemission and scanning tunneling spectroscopy.

I. INTRODUCTION

The quantitative experimental detection of surface-state energies on clean semiconductor surfaces has become possible in the last decade mostly by means of photoemission,[1] and also via optical[2] and energy-loss[3] techniques.

At present, these experimental results are being compared with very elaborate self-consistent one-electron calculations,[4–8] also in order to learn about the surface geometry, which is generally unknown. The implication is that effects not contained in one-electron calculations, e.g., of the local-density type, can be disregarded, an assumption which is not always obvious. While some work has been devoted towards many-body effects,[9–15] lattice-reconstruction effects,[9–16] and even surface electron-phonon coupling,[17] there seems to be no discussion available of polaron effects on surface states.

This paper is a first attempt to study the polaron effects produced by coupling of the surface-state electrons (and holes) to the vibrating surface lattice. For specificity, and also because of high current interest in it, we have chosen the clean Si(111)2×1 reconstructed surface as our working example. Since at least two widely discussed reconstruction models—the buckling model[18] and the chain model[19]—are available for the atomic structure of this surface, we have decided to consider both of them. This has been done also in the hope that our predicted behavior could be sufficiently different for the two cases so as to allow some conclusions to be drawn from a comparison of these predictions with existing or with future experiments. We stress again, however, that although most numerical calculations carried out in this paper refer to the 2×1 reconstructed Si(111) surface, our scope is much wider. We intend to discuss and illustrate the relevant concepts and the main consequences of the more general problem of the surface-state polaron, such as one could also find, for example, on a nonreconstructed surface or a metal surface.

The structure of this paper is as follows. We first construct the model Hamiltonian suitable for our purpose and fix the parameters used. This is done in Sec. II A for the buckling model and in Sec. III A for the chain model. Both our model Hamiltonians are strictly one-electron Hamiltonians, additionally involving coupling to a surface lattice. While, of course, electron-electron interactions may often be relevant in a real situation, they are not an essential ingredient of the physical effects we want to describe, and have thus been dropped. Two provisions must, however, be made in this respect. One is that the one-electron or hole states to be considered must always

be energetically close enough to the gap—or the Fermi energy in a metal—so that their lifetime, due in effect to electron-electron interactions,[20] is sufficiently long for any lattice relaxation to play a role. The second provision is that we will in fact reintroduce some effects of electron-electron interactions when dealing with electron-hole pairs bound to form an exciton. Of course, the electron-hole Coulomb attraction is not contained in our Hamiltonian and must be introduced separately to account for this important feature of the optical spectrum.[21,22] Calculations of such surface-state exciton binding energies and wave functions are carried out explicitly in Secs. II C and III C.

The energy shift and the lattice deformation that occurs when one extra electron—or one hole—is injected in a surface state, otherwise at equilibrium, are calculated for the two models in Secs. II B and III B. This state, i.e., a surface-state electron (hole) plus its accompanying surface-lattice deformation, is what we shall call a surface-state polaron.

A surface-state polaron will also build up around a bound electron-hole surface pair, i.e., a surface-state exciton. This situation, which typically occurs in optical absorption, is, of course, not just the linear superposition of the polarons of a free electron plus that of a free hole,[23–25] and requires separate calculations, which are carried out in Secs. II D and III D. The optical absorption itself is calculated—as it is perhaps the most important consequence of surface-state polarons of direct experimental relevance—in Secs. II E and III E.

The results of Secs. II and III show that surface-state polarons can have binding energies easily 1—2 orders of magnitude larger than those in the bulk of the same material. Thus, for example, the buckled Si(111)2×1 surface is a strong-coupling case with self-trapped electrons and holes—as in a bulk ionic crystal—while bulk Si is, of course, a case of weak coupling. Comparison between Secs. II and III, on the other hand, is useful in that it shows how critically dependent on the detailed surface situation the polaron effects can be, and how they can be handled in each case.

Finally, Sec. V is devoted to a discussion of situations where surface-state-polaron effects will, or might, play an important role. By analogy with known bulk situations, one would expect important consequences on (a) transport and (b) spectroscopy. Of these, transport is ruled out for a surface-state problem: no known evidence has so far been produced for it. One is then left with polaron effects on surface-state spectroscopy. The most direct observation of polaron effects is expected in optical absorption from surface states. For increasing coupling strength, the nature of the absorption process goes from band to band (as in a bulk semiconductor) to Franck-Condon type (as in a color center).[26,27] This aspect is discussed in Sec. IV A. The corresponding effects expected on luminescence are briefly discussed in Sec. IV B, particularly in connection with the contrasting behavior of the two models investigated. The remaining subsections, IV C—IV E, are devoted to speculations about possible new experimental consequences of surface-state polarons. The ideas elucidated in this last part are totally qualitative, and may or may not turn out to have actual quantitative relevance.

II. SURFACE-STATE POLARONS IN THE BUCKLING MODEL OF Si(111)2×1

In the following series of subsections, II A—II E, we introduce and study polarons in a semiconductor surface state. This will be done in the following sequence. First, we introduce a one-electron Hamiltonian describing the chosen model, i.e., that of a Si(111)2×1 buckled surface. Then we study an electron or a hole in a surface state and determine (a) the form and magnitude of the accompanying lattice distortion, and (b) the energy shift (polaron binding) caused by this distortion. Lastly, we consider, in the same context, a surface electron-hole pair and the resulting optical-absorption line shape, as modified by lattice relaxation.

A. The buckling model and its parameters

The surface geometry for the buckling model of Si(111)-2×1 (Ref. 18) is shown in Fig. 1. Alternate $[1\bar{1}0]$ rows of surface atoms are displaced in and out with respect to the "ideal" geometry. The outermost atomic layer of each surface unit cell (a cell is labeled by the index n) contains one raised atom [labeled $(n,1)$] and one lowered atom [labeled $(n,2)$]. Each surface atom carries a dangling-bond (DB) orbital, which we denote $|n,i\rangle$ $(i=1,2)$. As it turns out,[4–9,28] the surface states of Si(111) with energies close to the Fermi level have a very strong DB character. Thus it is reasonable to restrict our attention to DB orbitals in this case. The simplest picture of a DB is a combination of s and p_z wave functions, with coefficients which depend on the distance H_{ni} of the atom from the second atomic plane,

$$|n,i\rangle=\sqrt{6}\frac{H_{ni}}{a}|s,i\rangle+\left[1-6\left[\frac{H_{ni}}{a}\right]^2\right]^{1/2}|p_z,i\rangle\ , \quad (2.1)$$

where a is the surface lattice constant ($a=3.85$ Å). With the choice (2.1), $|n,i\rangle$ is an sp^3 orbital when $H_{ni}=H_0=a/2\sqrt{6}$ (the value for the "ideal" geometry), while it reduces (a) to a p_z orbital for the fully relaxed case $H_{ni}=0$, and (b) to a pure s orbital when

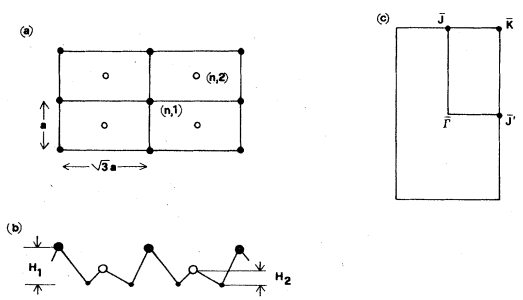

FIG. 1. Geometrical arrangement of surface atoms for the buckling model of Si(111)2×1. Solid and open circles represent raised and lowered first-layer atoms, respectively. (a) Top view, $a=3.85$ Å is the surface lattice constant along the $[1\bar{1}0]$ direction. (b) Side view, H_1 and H_2 are the vertical distances of the raised and lowered atoms from the second atomic plane (not in scale). (c) Surface Brillouin zone.

$H_{ni}=2H_0=a/\sqrt{6}$, for then the angle between each pair of backbonds is $\pi/2$. The DB energy depends on atomic position, in the form

$$\epsilon_i(H_{ni})=\epsilon_p-\frac{C}{2}\left[\frac{H_{ni}}{a}\right]^2, \tag{2.2}$$

where $C=12(\epsilon_p-\epsilon_s)$, and ϵ_s and ϵ_p are the s and p atomic energies.

As mentioned in the Introduction, we do not intend to include electron-electron interactions in our calculation (except when dealing with the exciton problem). In particular, for instance, the electronic part of the total energy will be simply calculated as a sum of one-electron energies. The possible relevance of many-body effects in buckling-type models has been discussed to some extent in a few papers,[10–15] and has been found to be important in the determination of the relative stability of various surface configurations (e.g., paramagnetic versus antiferromagnetic[13]). Our point here is, however, to start with the simplest possible scheme that would enable us to focus on surface-state polarons, a one-electron effect. Thus we just assume in this section that the buckled nonmagnetic surface is the stable ground-state configuration of Si(111)2×1, and we describe single-particle properties by the model surface-state Hamiltonian:

$$\mathscr{H}=\sum_{n,i}\epsilon_i(H_{ni})\,|\,n,i\rangle\langle n,i\,|+t\sum_{\langle ni,mj\rangle}(\,|\,n,i\rangle\langle m,j\,|+\text{H.c.}), \tag{2.3}$$

where t is the hopping integral, and $\langle ni,mj\rangle$ indicates a restriction to nearest neighbors. Here electron-lattice coupling is present through the dependence (2.2) of the on-site energy on the atom z coordinate H_{ni}. We wish to emphasize that this is by no means the only electron–surface-lattice coupling mechanism to be expected in a real situation. For example, (2.3) does not include the electrostatic coupling (Fröhlich type[29]) that might quantitatively play a role in this case, since the buckled surface is strongly ionic. Restriction to the coupling (2.3) helps greatly to simplify the problem, while in our view it should not lead to important qualitative errors. Quantitatively, we expect (2.3) to somewhat underestimate the coupling strength and thus the polaron binding energies.

For static and uniform buckling, i.e., $\epsilon_i(H_{ni})\equiv\epsilon_i$ ($i=1,2$), the eigenvalues of (2.3) become

$$E_\pm(\vec{k})=\frac{\epsilon_1+\epsilon_2}{2}+2t\cos(\vec{k}\cdot\vec{a}_2)\pm\left[\left[\frac{\epsilon_2-\epsilon_1}{2}\right]^2+\left[4t\cos\frac{\vec{k}\cdot\vec{a}_1}{2}\cos\frac{\vec{k}\cdot\vec{a}_2}{2}\right]^2\right]^{1/2}, \tag{2.4}$$

where $\vec{k}$ is a vector of the two-dimensional surface Brillouin zone (SBZ) of Fig. 1(c), and $\vec{a}_1=\sqrt{3}a\hat{x}$ and $\vec{a}_2=a\hat{y}$. The lower and upper signs in (2.4) refer to the filled (−), or lower band, and to the empty (+), or upper band, respectively. We must now provide an estimate of the parameters t, ϵ_1, and ϵ_2 for Si(111)2×1. The results of several calculations have shown that the width of the DB bands for the buckling model is quite small, typically a few tenths of an electron volt.[4,5,28] This is partly due to the large separation between surface atoms, nearest neighbors on the surface being bulk second neighbors, but also to a strong cancellation effect.[30] While the direct hopping has a negative sign, there is an indirect hopping term via second-layer atoms that is of opposite sign and slightly larger in magnitude. The latter is sufficiently large to offset the former, but the ensuing cancellation makes the surface band of Si(111) particularly narrow. Assuming thus that $t>0$, the width of the lower band in our model band structure is $B_-=4t$. We take $t=0.075$ eV, resulting in $B_-=0.3$ eV, a value in the range of current estimates. The appropriate value of $\epsilon_2-\epsilon_1$, on the other hand, can be determined *a posteriori,* by requiring that the calculated absorption peak position fit the experimental value,[2] $\hbar\omega\sim0.45$ eV. This requires, as will be shown later, $\epsilon_2-\epsilon_1\sim1$ eV. With these parameters our model band structure (2.4) is shown in Fig. 2. A useful dimensionless parameter that characterizes it is

$$\alpha\equiv t/(\epsilon_2-\epsilon_1), \tag{2.5}$$

which is much smaller than unity in the present case, and will be later used as an expansion parameter.

It is desirable at this point to introduce the Wannier functions of this problem. The Wannier states will be useful in the derivation of a simple expression for the total energy, and also as good basis functions for the polaron states. The Wannier functions of our model can be expressed as

$$a_{\pm n}=\sum_m[c_{1\pm}(n-m)\,|\,m,1\rangle+c_{2\pm}(n-m)\,|\,m,2\rangle], \tag{2.6}$$

where the $c_{i\pm}$'s are calculated using the Bloch eigenstates corresponding to (2.4). The general expression for $a_{\pm n}$ is quite involved. However, we can exploit the fact that the "gap" $(\epsilon_2-\epsilon_1)$ is sufficiently larger here than the bandwidth $(4t)$, and expand to lowest order in α. Then the functions $a_{\pm n}$ take the form

$$a_{-n}=|\,n,1\rangle+\alpha\sum_{\langle m2,n1\rangle}|\,m,2\rangle, \tag{2.7}$$

$$a_{+n}=|\,n,2\rangle+\alpha\sum_{\langle m1,n2\rangle}|\,m,1\rangle, \tag{2.8}$$

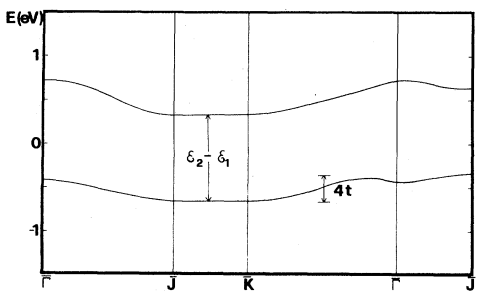

FIG. 2. Surface-state energy bands for the buckling model of Si(111)2×1, with $\epsilon_2-\epsilon_1=0.98$ eV and $t=0.075$ eV. The zero of the energy scale is the midgap energy.

where $\langle m2,n1\rangle$ ($\langle m1,n2\rangle$) indicates the four nearest neighbors of type 2 (1) surrounding the atom $(n,1)$ $[(n,2)]$. With our value $\alpha=0.077$, the lower (upper) Wannier state essentially consists exclusively of the DB orbital on atom 1 (2), with only a 2.2% admixture of atom 2 (1). This means, of course, that the surface is strongly ionic, the electronic charge being almost completely localized on type-1 atoms.[31] The Wannier-state energies are

$$\epsilon_{-n}=\epsilon_1-4t\alpha\ , \tag{2.9}$$

$$\epsilon_{+n}=\epsilon_2+4t\alpha\ , \tag{2.10}$$

the difference $E_{gn}=(\epsilon_2-\epsilon_1)+8t\alpha$ being the single-particle gap for localized states.

We now want to determine the $T=0$ K static equilibrium positions of the surface atoms corresponding to the Hamiltonian (2.3) and the chosen values of the parameters. Thus we minimize the total energy of our model system, consisting of $2N$ surface atoms and $2N$ surface electrons, if N is the number of surface unit cells. Within the usual Born-Oppenheimer approximation, the total energy is approximately given by

$$\mathscr{E}_{2N}=\tfrac{1}{2}\sum_{n,i}\gamma(H_{ni}-H_0')^2+2\sum_n\epsilon_{-n}\ , \tag{2.11}$$

where $H_{ni}-H_0'$ is the displacement of the atom (n,i) from an appropriate reference value H_0', which will be discussed below, and γ is some effective elastic force constant for atomic displacements perpendicular to the surface plane, therefore simulating the effect of stretching and bending the backbonds from their equilibrium configuration. In the ground state all unit cells are equivalent, and we normalize our total energy per unit cell,

$$\mathscr{E}(H_1,H_2)=\tfrac{1}{2}\gamma[(H_1-H_0')^2+(H_2-H_0')^2]+2\left[\epsilon_1(H_1)-\frac{4t^2}{\epsilon_2(H_2)-\epsilon_1(H_1)}\right], \tag{2.12}$$

where ϵ_1 and ϵ_2 depend on H_1 and H_2 through (2.2). Minimizing $\mathscr{E}$ with respect to H_1 and H_2, we find

$$H_1^g=\frac{\gamma a^2H_0'}{\gamma a^2-(2-8\alpha^2)C}\ , \tag{2.13a}$$

$$H_2^g=\frac{\gamma a^2H_0'}{\gamma a^2-8\alpha^2C}\ . \tag{2.13b}$$

Note that $2-8\alpha^2$ and $8\alpha^2$ are the fractions of electronic charge on atom 1 and 2, respectively. Equations (2.13) show that when the height H_i of an atom increases, so does the electronic charge on it. In fact, this is due to the dehybridization effects contained in (2.1) and (2.2) which cause ϵ_1 to decrease with increasing H_i. In particular, it is clear from (2.13) that H_0' would be the atomic position if the DB's were empty. An estimate for the numerical values of the parameters C, γ, and H_0' are $C=52.8$ eV, $\gamma=20.4$ eV Å^{-2}, and $H_0'=0.65$ Å, as discussed in Appendix A. Along with these values, the equilibrium positions (2.13) of the buckled surface are $H_1^g=0.99$ Å and $H_2^g=0.66$ Å.

Since H_1^g and H_2^g minimize the energy (2.12), it follows that substitution of $H_1=H_1^g+q_1$ and $H_2=H_2^g+q_2$ transforms $\mathscr{E}$ in a quadratic form in q_1 and q_2. To lowest order in α, the two vibrational normal-mode frequencies are

$$\omega_1\cong[(\gamma a^2-2C)/Ma^2]^{1/2},\quad \omega_2\cong(\gamma/M)^{1/2}\ . \tag{2.14}$$

The corresponding eigenvectors show them to consist essentially of a local vertical vibration of atoms 1 and 2, respectively. We note that the frequency of atom 2 in this approximation is identical to that in the hypothetical "empty" surface ($\hbar\omega_2=55$ meV), while that of atom 1 is lowered ($\hbar\omega_1=44$ meV) by the presence of two electrons.

B. Electron polaron and hole polaron

Different techniques are available to handle weak-coupling (WC) and strong-coupling (SC) polarons.[32] Therefore, we should first recognize whether our surface-state problem is WC, SC, or intermediate. This will be done in the following way.

We start by considering an extra electron added to the system of $2N$ surface atoms and $2N$ electrons. In the absence of coupling to the lattice, the excess electron is in a Bloch state of the empty upper band. When the coupling to the lattice is turned on, the electron is subject to two competing tendencies: one toward delocalization, so as to minimize the kinetic energy, and local lattice distortions, which reduce the electron on-site energy and tend to favor the localized situation. The strength of the localizing force is measured by the relaxation energy E_R^e which is released when the lattice is allowed to distort around a localized electron.[26] More precisely, E_R^e is the difference between the total energies $\mathscr{E}_{2N+1}$ of the system of $2N$ atoms and $2N+1$ electrons before and after lattice relaxation. If we express the wave function ψ_e of the excess electron as a linear combination of empty Wannier states,

$$\psi_e=\sum_n c_n a_{+n}\ , \tag{2.15}$$

the energy $\mathscr{E}_{2N+1}$ is a functional of both the set of atomic coordinates $\{H_{ni}\}$ and the set of coefficients $\{c_n\}$, $\mathscr{E}_{2N+1}(\{H_{ni}\},\{c_n\})$. Thus the relaxation energy is

$$E_R^e=\mathscr{E}_{2N+1}(\{H_{ni}^g\},\{c_n^g\})-\mathscr{E}_{2N+1}(\{H_{ni}^e\},\{c_n^e\})\ , \tag{2.16}$$

where the indices g and e label ground and relaxed values, respectively. Let us now tentatively assume that we are in a strong-coupling situation, so that the Born-Oppenheimer approximation is good. In this case the energy of the relaxed state can be calculated according to the adiabatic prescription: For any given configuration $\{H_{ni}\}$, first minimize $\mathscr{E}_{2N+1}$ with respect to $\{c_n\}$ in order to determine the adiabatic potential $\mathscr{E}(\{H_{ni}\},\{c_n(H_{ni})\})$, which can subsequently be minimized to determine H_{ni}^e. Even after elimination of the electronic coordinates, the problem of determining the infinite set of atomic coordinates $\{H_{ni}^e\}$ is still generally very difficult. For our SC situation, however, the following approximate procedure turns out to be convenient. We start by assuming that the electron is perfectly localized in a single unit cell, which we call 0,

$$c_n = \begin{cases} 1 & \text{if } n=0\,, \\ 0 & \text{otherwise}\,, \end{cases} \tag{2.17}$$

and calculate the value of E_R^e for this test case. This value must be compared with the corresponding kinetic energy B, that is, the energy released when the electron, initially localized in one unit cell, is allowed to spread throughout the surface lattice.[26] Here, B is the difference between the upper-Wannier-state energy ϵ_{+0} and the energy of the bottom of the upper band. If $E_R^e \gtrsim B$, we can consider (2.17) a sufficiently good guess. If, on the other hand, E_R^e should turn out to be noticeably smaller than B, then we must allow the electron to spread over successive shells of empty Wannier states. Eventually, if the linear size of the region in which $\{H_{ni}^e\}$ differs significantly from $\{H_{ni}^g\}$ becomes much larger than the lattice constant, our initial SC assumption (i.e., Born-Oppenheimer) will be invalid, and a different approximation scheme should then be used.

For our buckled-surface model, (2.15) with (2.17) turns out to be a good wave function for the excess electron, as will be shown below. This could, in fact, be anticipated since the Hamiltonian matrix element between neighboring Wannier functions is of order $\alpha \ll 1$, implying precisely that that electron spreading away from the central cell is small.

1. Electron polaron

The bandwidth B defined above must be calculated assuming that the surface lattice is frozen in the ground-state equilibrium configuration $H_1 = H_1^g$ and $H_2 = H_2^g$, with $H_1^g = 0.99$ Å and $H_2^g = 0.66$ Å. The upper-band minimum of (2.4) occurs at the $\bar{J}$ point $(0, \pi/a)$ of the SBZ (see Fig. 2) and is $\epsilon_2 - 2t$. The corresponding Wannier energy ϵ_{+0} is given by (2.10), yielding $B = 2t + 4t\alpha$, that is, $B = 0.17$ eV with our choice of the parameters.

The relaxation energy E_R^e is defined by (2.16). However, with our choice (2.15)–(2.17) of the electron wave function, the total adiabatic energy $\mathscr{E}_{2N+1}$ depends only on the set of atomic coordinates $\{H_{ni}\}$,

$$\mathscr{E}_{2N+1}(\{H_{ni}\}) = \tfrac{1}{2}\gamma \sum_{n,i} (H_{ni} - H_0')^2 + 2\sum_n \epsilon_{-n}(\{H_{ni}\}) + \epsilon_{+0}(\{H_{ni}\})\,, \tag{2.18}$$

where ϵ_{-n} is the energy of filled states in cell "n," while ϵ_{+0} is the energy of the extra electron in the cell "0." As described in Sec. II A the upper Wannier state a_{+0} is basically localized on the atom (0,2), with only a small spread on the four nearest neighbors of type 1. This implies, however, that even with the simplifying assumption (2.17), the lattice relaxation will, in principle, affect not only the atom (0,2) but also the neighboring atoms. This, in turn, alters the energies of their (filled) Wannier states. In this way the relaxation can propagate out to successive shells of neighbors. However, the relaxation amplitude decreases very quickly with increasing distance from the central site.[33] In this calculation we tentatively assume that there is no relaxation beyond the first shell of type-1 neighbors of the atom (0,2) [see Fig. 3(a)]. Taking into account the equivalence of these four neighbors, the relevant energy to be minimized is

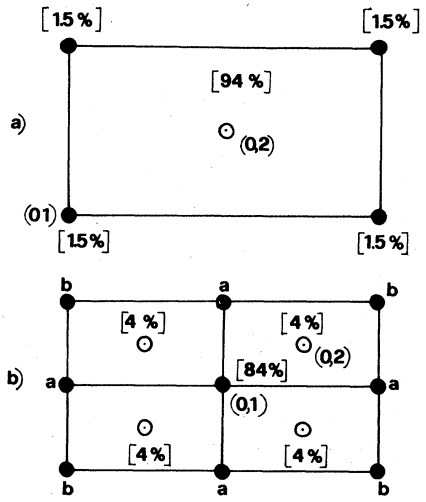

FIG. 3. Surface atoms involved in the relaxation following injection of (a) an excess electron in (0,2) and (b) an excess hole in (0,1). The values in square brackets denote the electron (hole) wave-function square amplitude at the various sites after relaxation.

$$\begin{aligned} \mathscr{E}(H_{01}, H_{02}) = {} & \tfrac{1}{2}\gamma[(H_{02} - H_0')^2 + 4(H_{01} - H_0')^2] \\ & + 8[\epsilon_1(H_{01}) - 3t\alpha_e' - t\alpha_e] \\ & + \epsilon_2(H_{02}) + 4t\alpha_e\,, \end{aligned} \tag{2.19}$$

where

$$\alpha_e' = \frac{t}{\epsilon_2(H_2^g) - \epsilon_1(H_{01})} \tag{2.20a}$$

and

$$\alpha_e = \frac{t}{\epsilon_2(H_{02}) - \epsilon_1(H_{01})}\,. \tag{2.20b}$$

The new local equilibrium positions for the atom (0,2) and its neighbors are

$$\begin{aligned} H_{01}^e &= \frac{\gamma a^2 H_0'}{\gamma a^2 - C(2 - \alpha_e^2 - 6\alpha_e'^2)}\,, \\ H_{02}^e &= \frac{\gamma a^2 H_0'}{\gamma a^2 - C(1 + 4\alpha_e^2)}\,. \end{aligned} \tag{2.21}$$

Numerically, the central-atom relaxation is quite large: from $H_2^g = 0.66$ Å to $H_{02}^e = 0.80$ Å. The corresponding relaxation of the four type-1 neighbors turns out to be, in fact, negligible, i.e., from $H_1^g = 0.990$ Å to $H_{01}^e = 0.988$ Å. This finding confirms the validity of our initial SC assumption. The relaxation energy amounts to $E_R^e = 0.15$ eV, resulting from an electronic energy gain of 0.32 eV—due to the outward displacement of the central atom—approximately half-balanced by the necessary elastic cost (-0.17 eV).[34] This relaxation energy E_R^e is almost identical to the bandwidth B (~ 0.17 eV), thus confirming once more that we are dealing with a strong-coupling case. We

can also calculate the mass renormalization for the excess electron. The renormalization factor is usually expressed as $\exp(S_e)$, where S_e is the Huang-Rhys factor,[26,27] given in our case (and $T=0$ K) by

$$S_e \equiv -2\ln\langle \chi^g_{\rm vib} \mid \chi^e_{\rm vib}\rangle = \sum_{i=1}^{2} \frac{M\omega_i^g\omega_i^e(H_i^g-H_i^e)^2}{\hbar(\omega_i^g+\omega_i^e)} . \tag{2.22}$$

Here, the $\chi_{\rm vib}$ are zero-point vibrational states, ω_1^g and ω_2^g are the vibrational frequencies in the ground state of the system with $2N$ electrons, given by (2.14), while ω_1^e and ω_2^e are the corresponding local frequencies in the relaxed state with an extra electron. The latter are calculated by expanding the adiabatic potential (2.19) around the equilibrium positions (2.21), which gives $\omega_1^e=44$ meV and $\omega_2^e=50$ meV (as opposed to $\omega_1^g=44$ meV and $\omega_2^g=55$ meV). The resulting value for the Huang-Rhys factor is $S_e=3.6$, which corresponds to a mass-enhancement factor $\exp(S_e)\sim 40$ for the excess electron. The original bandwidth $B=0.17$ eV is reduced to a few milli-electron-volts, showing that the electron can in fact be considered immobile and essentially classical.

2. Hole polaron

The same approach discussed for the case of an excess electron can be straightforwardly used to evaluate the relaxation energy E_R^h around a localized excess hole. Again, assume that the hole is perfectly localized in a single unit cell, which we call 0; thus its wave function ψ_h reduces to $\psi_h=a_{-0}$, the lower Wannier state of cell 0. The total adiabatic energy $\mathscr{E}_{2N-1}$ is a functional of only the atomic coordinates $\{H_{ni}\}$, and the relaxation energy can then be expressed as

$$E_R^h = \mathscr{E}_{2N-1}(\{H_{ni}^g\}) - \mathscr{E}_{2N-1}(\{H_{ni}^h\}) , \tag{2.23}$$

where

$$\mathscr{E}_{2N-1}(\{H_{ni}\}) = \tfrac{1}{2}\gamma\sum_{n,i}(H_{ni}-H_0')^2 + 2\sum_{n(\neq 0)}\epsilon_{-n}(\{H_{ni}\}) + \epsilon_{-0}(\{H_{ni}\}) . \tag{2.24}$$

In (2.23) the index h is used to label quantities of the hole relaxed state. As discussed in the preceding subsection, the lattice can, in principle, spread over a large region of the surface lattice because the Wannier functions are not strictly "single site." We tentatively assume that only the central atom (0,1) and its four type-2 nearest neighbors can relax. In this case, and taking into account the equivalence of the four type-2 atoms, the relevant part of the total energy is

$$\mathscr{E}(H_{01},H_{02}) = \tfrac{1}{2}\gamma[(H_{01}-H_0')^2+4(H_{02}-H_0')^2] + 8[\epsilon_1(H_1^g)-2t\alpha-2t\alpha_h'] + 8[\epsilon_1(H_1^g)-3t\alpha-t\alpha_h'] + \epsilon_1(H_{01})-4t\alpha_h , \tag{2.25}$$

where

$$\alpha_h' = \frac{t}{\epsilon_2(H_{02})-\epsilon_1(H_1^g)} \tag{2.26a}$$

and

$$\alpha_h = \frac{t}{\epsilon_2(H_{02})-\epsilon_1(H_{01})} . \tag{2.26b}$$

In (2.25),

$$\epsilon_{-a} \equiv \epsilon_1(H_1^g)-2t\alpha-2t\alpha_h'$$

and

$$\epsilon_{-b} \equiv \epsilon_1(H_1^g)-3t\alpha-t\alpha_h'$$

are the energies of the lower Wannier functions centered on the atoms denoted a and b, respectively, in Fig. 3(b). Minimization of (2.25) yields the new local equilibrium positions,

$$H_{01}^h = \frac{\gamma a^2 H_0'}{\gamma a^2 - C(1-4\alpha_h^2)} , \tag{2.27a}$$

$$H_{02}^h = \frac{\gamma a^2 H_0'}{\gamma a^2 - C(\alpha_h^2+6\alpha_h'^2)} . \tag{2.27b}$$

The numerical values of H_{01}^h and H_{02}^h are $H_{01}^h=0.76$ Å ($H_1^g=0.99$ Å) and $H_{02}^h=0.65$ Å ($H_2^g=0.66$ Å). As for the electron polaron, the relaxation is strong for the atom in the central site, but almost negligible for the neighboring atoms, thus supporting the initial SC assumption. Note that the sign of the relaxation for the central atom is the opposite of that of an excess electron. The energy balance now consists of a strong gain of elastic energy (-1.04 eV) partially cancelled by an increase of electronic energy ($+0.66$ eV). The resulting value for the hole relaxation energy is $E_R^h=0.38$ eV. This must be compared with the value for B_h, the kinetic energy of localization of the hole. B_h is the difference between the energy of the lower Wannier function and the top of the lower band in the undistorted lattice, $B_h=2t+4t\alpha=0.17$ eV in our case. Therefore we conclude that the hole should be self-trapped. This is confirmed by the value of the Huang-Rhys factor S_h, for which we find, using an expression analogous to (2.22), $S_h=8.3$ (the local vibrational frequencies in the relaxed state are now $\omega_1^h=51$ meV and $\omega_2^h=55$ meV). The resulting enhancement factor for the hole mass is $\exp(S_h)\sim 4000$, and the hole can thus be rather accurately described as a localized defect.

C. Exciton states in the buckling model

As a first step for the calculation of the optical spectrum, in this subsection we start studying electron-hole–pair excitations—namely exciton states—of our model system of $2N$ surface atoms and $2N$ electrons, assuming for the moment that the lattice is frozen in the ground-state equilibrium configuration. To this end we must introduce some effects of electron-electron interac-

tions which are so far not present in our calculations. Our model for the exciton consists of an electron transferred from a Wannier state of the lower band—basically localized on an atom of type 1—to an empty Wannier state centered on a nearest-neighbor atom of type 2. The justification for this model is that (a) this is certainly the lowest (singlet) exciton state, as suggested by the analogy with strongly ionic bulk materials, and (b) the dipole matrix element $\langle a_{-n} | \vec{r} | a_{+m} \rangle$—determining the strength of optical transitions—is nonvanishing only if a_{-n} and a_{+m} are first neighboring sites. In our calculation of the exciton binding energy, we shall also neglect the terms responsible for the exciton propagation through the surface lattice.[21] In our model, these terms—roughly proportional to the square of α in Eq. (2.5)—are very small. In addition, as shown by the results of the next subsection, the coupling to the lattice will cause self-trapping of the exciton. With this simplification, the singlet exciton binding energy E_{BS} reduces to the sum of the e-h Coulomb and exchange energies,[21]

$$E_{BS}=V_C-2V_x \ , \tag{2.28}$$

where

$$V_C=\int d^3r\, d^3r'\, a^*_{-0}(\vec{r})a_{-0}(\vec{r}) \times\frac{e^2}{\epsilon_s\,|\,\vec{r}-\vec{r}'\,|}a^*_{+0}(\vec{r}')a_{+0}(\vec{r}') \tag{2.29}$$

and

$$V_x=\int d^3r\, d^3r' a^*_{-0}(\vec{r})a_{+0}(\vec{r}) \times\frac{e^2}{\epsilon_{bg}\,|\,\vec{r}-\vec{r}'\,|}a^*_{+0}(\vec{r}')a_{-0}(\vec{r}') \ . \tag{2.30}$$

The binding energy of the triplet exciton, instead, is unaffected by electron-hole exchange, i.e., $E_{BT}=V_C$. The surface electron-hole exchange (2.30) is screened by the underlying bulk only, whereas the dielectric screening of the Coulomb attraction (2.29) contains also, in principle, the screening contribution of the surface states themselves.[35] However, introduction of this two-dimensional screening appears to be a minor correction in the present case, where the main interaction to be screened is intracell and will be approximately omitted. On the other hand, we will take care to include it in the π-bonded chain model, where the exciton radius is somewhat larger.

In conclusion, we take the image-charge screening $\epsilon_s=\epsilon_{bg}=(\epsilon_b+1)/2$ for both V_C and V_x, where ϵ_b is the bulk dielectric constant ($\epsilon_b\approx 12$ for Si). Using the expansion (2.6) of the Wannier functions in terms of DB orbitals, (2.29) and (2.30) can be expressed in terms of intrasite,

$$U_i=\int d^3r\, d^3r'\,|\,\varphi_i(\vec{r})\,|^2\frac{e^2}{\epsilon'_{bg}\,|\,\vec{r}-\vec{r}'\,|}\,|\,\varphi_i(\vec{r}')\,|^2 \ ,$$

and intersite,

$$V_{ij}(R)=\int d^3r\, d^3r'\,|\,\varphi_i(\vec{r})\,|^2\frac{e^2}{\epsilon_{bg}\,|\,\vec{r}-\vec{r}'\,|}\,|\,\varphi_j(\vec{r}'-\vec{R})\,|^2 \ , \qquad i=1,2;\ \vec{R}\neq\vec{0}$$

Coulomb interactions. The intrasite background screening ϵ'_{bg} appearing in U_i is very difficult to evaluate, and we have chosen to make it equal to the intersite screening $\epsilon'_{bg}=\epsilon_{bg}$. We evaluate $V_{ij}(R)$ using the point-charge approximation,

$$V_{ij}(R)\sim\frac{e^2}{\epsilon_{bg}R} \ ,$$

which is justified by the relatively large distances between surface atoms and by the lateral localization of DB states.[4–6] The intrasite repulsion U_i is evaluated numerically using tabulated atomic wave functions.[36] We ignore the different hybridization of the two DB's, and obtain $U=1.9$ eV for sp^3 hybrids. This value is in the range of current estimates of the intrasite repulsion for silicon.[37]

The exciton binding energy (2.28) can be explicitly written as

$$E_{BS}=-2\alpha^2\beta^2U+(\beta^4+9\alpha^4+4\alpha^2\beta^2)V(\,|\,\tfrac{1}{2}\vec{a}_1+\tfrac{1}{2}\vec{a}_2\,|\,)+2\alpha^2\beta^2[V(\,|\,\vec{a}_1\,|\,)+V(\,|\,\vec{a}_2\,|\,)+V(\,|\,\vec{a}_1+\vec{a}_2\,|\,)] +\alpha^4[3V(\,|\,\tfrac{3}{2}\vec{a}_1+\tfrac{1}{2}\vec{a}_2\,|\,)+3V(\,|\,\tfrac{1}{2}\vec{a}_1+\tfrac{3}{2}\vec{a}_2\,|\,)]+V(\,|\,\tfrac{3}{2}\vec{a}_1+\tfrac{3}{2}\vec{a}_2\,|\,) \ , \tag{2.31}$$

where α was defined in (2.5) and $\beta^2=1-4\alpha^2$ (recall that $\vec{a}_1=\sqrt{3}\,a\hat{x}$ and $\vec{a}_2=a\hat{y}$, as shown in Fig. 1). Numerically, we obtain $E_{BS}=0.55$ eV, that is, essentially, the Coulomb interaction between two point charges on nearest-neighbor sites. With the same parameters the triplet-state binding energy is $E_{BT}=0.57$ eV. The (electron-hole—exchange) singlet-triplet splitting obtained here is very small, essentially because it is a contact interaction, i.e., it is proportional to $|\,\psi(r_e=r_h)\,|^2$, and in our model the electron and the hole belong almost totally to the two different sites, (0,1) and (0,2), respectively, in the cell.

D. Exciton polaron

The presence of a surface-state electron-hole pair will also cause a surface-lattice distortion, just as a single excess electron or hole does. This relaxation affects the wave function of both particles, and hence, in principle, their binding energy as well. To study this effect we follow the same procedure of Sec. II B for the electron and hole polarons, including, however, the e-h interaction energy $\mathscr{E}_{e\text{-}h}$ as an essential ingredient of the relevant energy to be minimized:

$$\mathscr{E}=\mathscr{E}_{\text{elastic}}+\mathscr{E}_{\text{electronic}}+\mathscr{E}_{e\text{-}h} \ . \tag{2.32}$$

Our model for the exciton is the same studied in Sec. II C that is, basically, a hole on the atom $h\equiv(0,1)$ and an electron on the atom $e\equiv(0,2)$. As in the case of a single electron or hole, we assume that the only atoms which can relax are h, e, and their respective first neighbors, as shown in Fig. 4. The elastic energy is then (neglecting relaxation

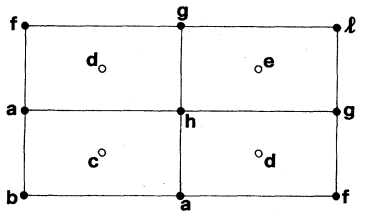

FIG. 4. Surface atoms involved in the relaxation following creation of an exciton, with the hole localized at h and the electron at e.

of atoms such as a and b, that are not first neighbors)

$$\mathscr{E}_{\text{elastic}}=\tfrac{1}{2}\gamma(h_h^2+h_e^2+h_c^2+2h_d^2+2h_g^2+h_l^2)\ , \qquad (2.33)$$

where we use the simplified notation $h_\nu=H_\nu-H_0'$ and the labeling of the various sites is given in Fig. 4. The part of the total electronic energy which can change by relaxation is

$$\mathscr{E}_{\text{electronic}}=\epsilon_{+0}+\epsilon_{-0}+4\epsilon_{-a}+2\epsilon_{-b}+4\epsilon_{-f}+4\epsilon_{-g}+2\epsilon_{-l}\ , \qquad (2.34)$$

where ϵ_{+0} and ϵ_{-0} are the energies of the upper (centered on e) and lower (centered on h) Wannier states of cell 0, while ϵ_{-a}, ϵ_{-b}, etc. are the energies of the lower Wannier states centered on the atoms a, b, etc. in Fig. 4. These Wannier energies have the same meaning and expressions as those given in the preceding subsections, e.g.,

$$\epsilon_{+0}=\epsilon_2(H_e)+\frac{t^2}{\epsilon_2(H_e)-\epsilon_1(H_h)}+\frac{2t^2}{\epsilon_2(H_e)-\epsilon_1(H_g)}+\frac{t^2}{\epsilon_2(H_e)-\epsilon_1(H_l)}\ ,$$

as can be easily inferred from Fig. 4. Finally, the electron-hole–interaction energy is approximated by a slightly simplified form of (2.31),

$$\mathscr{E}_{e\text{-}h}=2\alpha_{e\text{-}h}^2\beta_{e\text{-}h}^2U-(\alpha_{e\text{-}h}^4+\beta_{e\text{-}h}^4+4\alpha_{e\text{-}h}^2\beta_{e\text{-}h}^2)V(a)\ , \qquad (2.35)$$

where $\alpha_{e\text{-}h}^2$ and $\beta_{e\text{-}h}^2$ depend on the atomic coordinates of the atoms e and h through $\alpha_{e\text{-}h}^2=\frac{1}{2}(1-p)$ and $\beta_{e\text{-}h}^2=\frac{1}{2}(1+p)$, with

$$p=\left[1+\frac{4t^2}{[\epsilon_2(H_e)-\epsilon_1(H_h)]^2}\right]^{-1/2}\ .$$

Minimization of (2.32) with respect to $\{h_h,h_e,\ldots\}$—performed numerically—leads to the local equilibrium configuration given in Table I. As in the case of the single electron and single hole, there is a strong relaxation of the atoms in the central cell (outward and inward displacements for e and h, respectively), while all other atomic positions are substantially unaltered. Note that, due in part to the presence of the electron-hole–interaction term in (2.32), the magnitude of the displacement of the atom e (and, similarly, h) is smaller with respect to the single-electron (-hole) case. The relaxation energy E_R^{exc} around the localized exciton is obtained as the difference between the values taken by (2.32) before and after the relaxation. The numerical value for E_R^{exc} is $E_R^{\text{exc}}=0.34$ eV. The effective bandwidth B_{exc} for the exciton motion can be estimated as half of the bandwidth for the single electron or hole, i.e., $B_{\text{exc}}\sim 0.08$ eV in our case. This leads to the conclusion that the exciton polaron—as was the case for the hole polaron—is self-trapped. The energy-configuration diagram for the ground and excited states of our model system is sketched in Fig. 5. The vertical excitation energy is $\epsilon_0=E_g^0-E_{BS}^0$, where E_g^0 is the local single-particle gap and E_{BS}^0 is the singlet exciton binding energy in the unrelaxed lattice, numerically $\epsilon_0=0.47$ eV with our parametrization. This energy gives the position of the absorption peak according to the Franck-Condon principle, while E_R^{exc} is the energy released after the optical excitation.[26,27] For the emission process, the Franck-Condon energy ϵ_1 is given by $\epsilon_1=\epsilon_0-E_R^{\text{exc}}-\epsilon_2$, where ϵ_2 is the energy of the ground state with a distorted lattice configuration (see Fig. 5). Using the results of Table I we can calculate $\epsilon_2\simeq 0.12$, which yields $\epsilon_1\approx 0$ for the peak of the emission line, and, correspondingly, an extremely large Stokes shift, essentially equal to the Franck-Condon excitation energy. This is indicated in Fig. 5 by the minimum of the excited-energy curve essentially falling onto the ground-state-energy curve.

TABLE I. Vertical distance from the second atomic plane (in Å) of the surface atoms shown in Fig. 4, before and after the relaxation following creation of an exciton (with the electron at e and the hole at h). Also given for comparison are the relaxed atomic position for a single electron at e and a single hole at h. For the "ideal" Si(111) surface, the distance between the first and the second atomic planes is $H_0=0.79$ Å.

	H_e	H_h	H_c	H_d	H_g	H_l
Before relaxation	0.657	0.990	0.657	0.657	0.990	0.990
After relaxation (exciton)	0.727	0.860	0.658	0.658	0.990	0.990
After relaxation (electron)	0.801	0.988	0.657	0.657	0.988	0.988
After relaxation (hole)	0.653	0.765	0.653	0.653	0.990	0.990

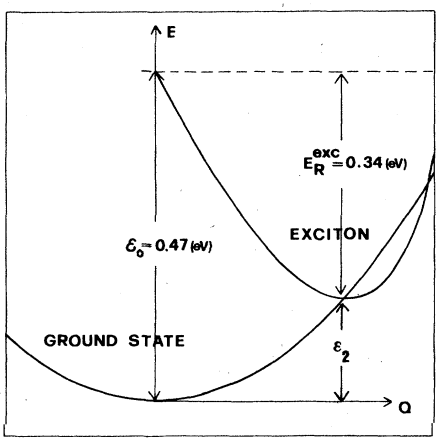

FIG. 5. Qualitative energy-configuration diagram for the ground state and the lowest singlet exciton of our buckling model of Si(111)2×1. $\epsilon_0=0.47$ eV is the position of the absorption peak according to the Franck-Condon principle, $E_R^{exc}=0.34$ eV is the energy released after optical excitation, and $\epsilon_1=\epsilon_0-(E_R^{exc}+\epsilon_2)\approx 0$ is where the luminescence line should be.

E. Absorption line shape

In the adiabatic and Condon approximation, the normalized line-shape function for transitions from the electronic ground state (g) to the exciton state (ex) can be written as[27]

$$I_{g,ex}(E)=I_0\sum_k P_k^g\sum_l |\langle\chi_k^g|\chi_l^{ex}\rangle|^2\delta(\epsilon_{ex,l}-\epsilon_{g,k}-E)\ , \tag{2.36}$$

where $|\chi_k^g\rangle$ and $|\chi_e^{ex}\rangle$ are the vibrational wave functions for the electronic ground and excited states, with total quantum numbers k and l, respectively. P_k^g is the probability of the state $|\chi_k^g\rangle$ at thermal equilibrium, and I_0 is the optical (electronic) squared matrix element.

The phonon frequencies in the ground electronic state are given in Sec. II A. In this case, atomic vibrations on sites of type 1 and 2 can be considered essentially uncoupled because of the small spread of valence electrons from type-1 atoms to neighboring sites. The ground-state vibronic wave functions are

$$|\chi_k^g\rangle=\prod_n\prod_{i=1}^{2}\chi_{k_{n,i}}^{(g)}(Q_{ni}-H_{ni}^g)\ , \tag{2.37}$$

where Q_{ni} and H_{ni}^g denote the actual coordinate and the equilibrium position of the atom (n,i), and $\chi_{k_{n,i}}^{(g)}$ is the wave function of a harmonic oscillator of frequency ω_i^g and quantum numbers $k_{n,i}$ (with $\sum_{ni}k_{ni}=k$).

When an exciton is created in the cell 0, the vibrational motions of the atoms on which the electron and the hole are centered become coupled through the e-h interaction. For small displacements from the equilibrium configuration, the adiabatic potential for the motion of the e and h atoms can be expressed in the form

$$\mathscr{E}=\tfrac{1}{2}\gamma_h(Q_h-H_h^{exc})^2+\tfrac{1}{2}\gamma_e(Q_e-H_e^{exc})^2 +\delta(Q_h-H_h^{exc})(Q_e-H_e^{exc})+\epsilon_2\ , \tag{2.38}$$

where the force constants γ_h, γ_e, and δ are, in principle, given by the respective second derivatives of (2.32), evaluated at $Q_h=H_h^{exc}$ and $Q_e=H_e^{exc}$. It turns out, however, that H_h^{exc} and H_e^{exc} are so very different from H_{01}^g and H_{02}^g of the ground state, that the true excited-state "potential energy" (2.32), which is very nonparabolic, is badly misrepresented, in the neighborhood of $Q_h=H_{n1}^g$ and $Q_e=H_{n2}^g$, by (2.38) if the values of γ_h, γ_e, and δ indicated above are used. Strictly speaking, one should determine numerically the true vibronic levels of (2.32), which would no longer be of harmonic-oscillator type. However, it is clear that we are only interested to know these excited vibronic states in the neighborhood of $Q_e=H_{n1}^g$ and $Q_h=H_{n2}^g$. Locally, these eigenstates will still be similar to harmonic-oscillator wave functions, but with different parameters. We have found that these wave functions are reasonably approximated by the harmonic eigenfunctions of (2.38), where, however, different values of the four constants γ_h', γ_e', δ', and ϵ_2' are used. We use $\gamma_h'=20.7$ eV/Å^2, $\gamma_e'=19.5$ eV/Å^2, $\delta'=3.1$ eV/Å^2, and $\epsilon_2'=0.24$ eV, which reasonably describe ϵ of (2.32) in the important region. The corresponding normal mode frequencies are $\hbar\omega_+=58.7$ meV and $\hbar\omega_-=50.2$ meV. The lower-frequency mode is characterized by the two atoms e and h vibrating in phase, while the higher-frequency mode has them vibrating out of phase. The frequency $\hbar\omega_-$ is close to the frequency characterizing the outward and inward relaxation of the unreconstructed surface in its ground electronic state, as calculated in Sec. II A. The other mode appears to be pushed up in energy because it involves changes of the electron-hole—interaction energy which itself is large. This is an example of how the presence of an exciton can *stiffen* the lattice rather than soften it. The vibrational wave functions for the electronic excited state are

$$|\chi_l^{ex}\rangle=\prod_{n\ (\neq 0)}\prod_{i=1}^{2}\chi_{l_{n,i}^+}^{(g)}(Q_{ni}-H_{ni})\chi_{l^+}^{(+)}(Q^+)\chi_{l^-}^{(-)}(Q^-)\ , \tag{2.39}$$

where Q^+ and Q^- are the normal-mode displacements from the equilibrium positions of the e and h atoms.

We have calculated the absorption line shape (2.36) numerically for increasing temperatures, with cutoff $k_{0,i}=l^{\pm}=10$ in the summations over initial and final vibronic states, and with an energy resolution $\Delta E=10$ meV. The results are displayed in Fig. 6 in the form of histograms, the vertical lines being approximately the zeros of the δ-function argument in (2.36). The main lines—determining the basic feature of the absorption line shape—are accompanied by satellites forming a fine structure which becomes increasingly richer with increasing temperature. The line-shape envelope is asymmetrical (Poisson-distribution-like) at low temperatures, and evolves slowly towards a Gaussian shape with increasing temperature, as in usual strong-coupling situations.[27]

At the lowest temperature ($T=2$ K) the absorption

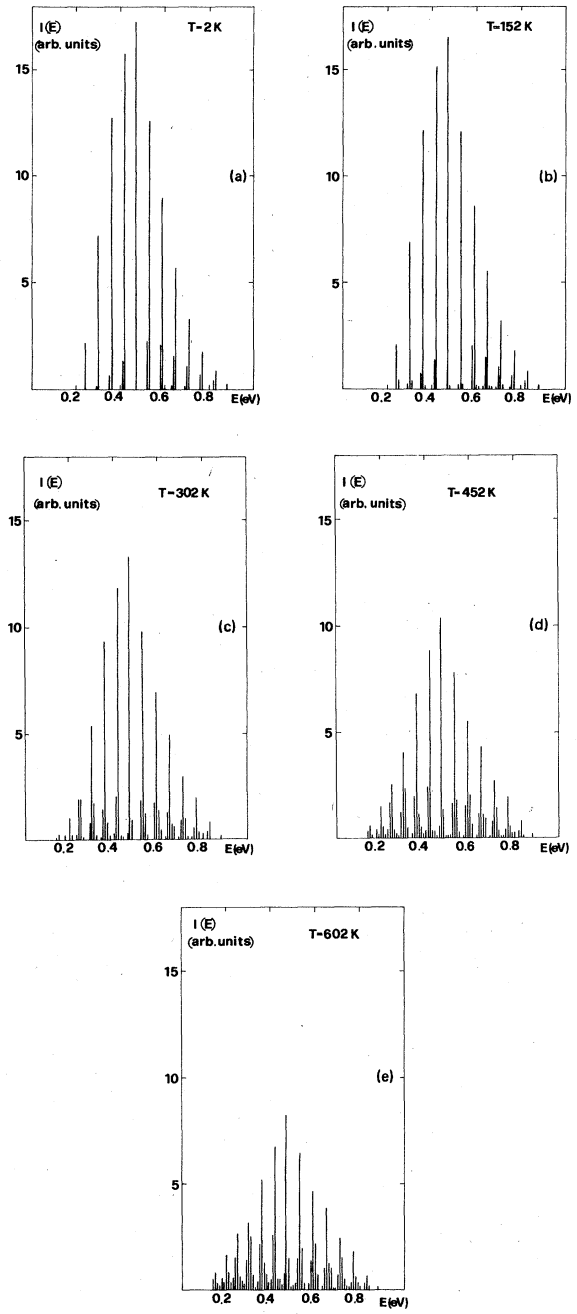

FIG. 6. Normalized absorption line shape at various temperatures for the buckling model of Si(111)2×1, in the Condon approximation. The width of each line of the histogram is $E=10$ meV. The modulations are due to two different vibrational frequencies of the excited state ($\hbar\omega_+=59$ meV and $\hbar\omega_-=50$ meV), as discussed in the text. Note that before these calculated line shapes can be compared with experiments, the additional rigid red shift due to the T dependence of the reconstruction magnitude discussed in Sec. IV A must be considered.

starts approximately at the energy ϵ_2', and has a fine structure due to the slight difference of $\hbar\omega_+$ and $\hbar\omega_-$. The peak of the absorption spectrum occurs at a frequency which is approximately the vertical excitation energy $\epsilon_0=0.47$ eV of Fig. 5.

With increasing temperature, the excited vibrational states of the initial electronic configuration give an increasing contribution to the absorption: This produces a tail on the low-energy side of the spectrum, while the fine-structure sidebands become more numerous and intense with respect to the main sidebands. The total oscillator strength remains constant, being transferred from the high spikes to the low spikes. The line shape becomes broader and more symmetrical, while there are no detectable shifts of the peak position within the accuracy of our calculations. We shall return to discuss this line shape in Sec. IV A.

III. SURFACE-STATE POLARONS IN THE π-BONDED CHAIN MODEL

In this section we shall study surface-state polarons for the π-bonded (dimerized-) chain model of Si(111)2×1 recently proposed by Pandey.[19] We follow closely the scheme used in Sec. II for the buckling model. In Sec. III A we introduce our one-electron Hamiltonian, fix its parameters by requiring a reasonable comparison of the resulting band structure with known experimental results, and finally determine the corresponding equilibrium positions (dimerization amplitude) of the surface atoms. In Sec. III B we study polaron states associated with an excess carrier—electron or hole—in a surface state. In Secs. III C—III E we consider an electron-hole pair as created, for instance, by optical excitation. For this we first study the exciton binding energy and wave function in the frozen lattice (Sec. III C), and next the coupling of the exciton to phonons (Sec. III D). Finally, we calculate (Sec. III E) the absorption line shape.

A. The model and the parameters

In the π-bonded chain model[19] the surface atoms are each bonded to two other surface atoms and form zigzag chains along the $[1\bar{1}0]$ direction similar to those occurring on the Si(110) surface. An important feature of this geometry is that the surface atoms along a chain are as close as bulk nearest neighbors ($d_b=2.35$ Å), while different chains are quite well separated, their distance being ~ 6.7 Å. Because of this anisotropy the model has a large dispersion[7,8,19] of the DB bands along the chain direction $\bar{\Gamma}\bar{J}$, and flat bands along $\bar{J}\bar{K}$ and $\bar{\Gamma}\bar{J}'$, perpendicular to the chains.

As was done for the buckling model in Sec. II, we focus only on the atoms of the outermost atomic plane and consider the DB-like states, which we assume to be mostly p_z in this case. Within this approach, the symmetric chain model originally proposed for Si(111)2×1 has degenerate bands along $\bar{J}\bar{K}$. To remove this degeneracy we assume that the ground-state configuration of the surface is characterized by uniformly dimerized chains, with alternating short (contracted) and long (stretched) bonds.[38] The situation is thus very similar to that of a Peierls-distorted quasi-one-dimensional system, particularly polyacetylene.[39] As shown by Fig. 7, the dimerization breaks the reflection symmetry through the x-z plane and this gives rise to a finite gap along $\bar{J}\bar{K}$. Contrary to the buckling model, no charge transfer occurs between DB's,

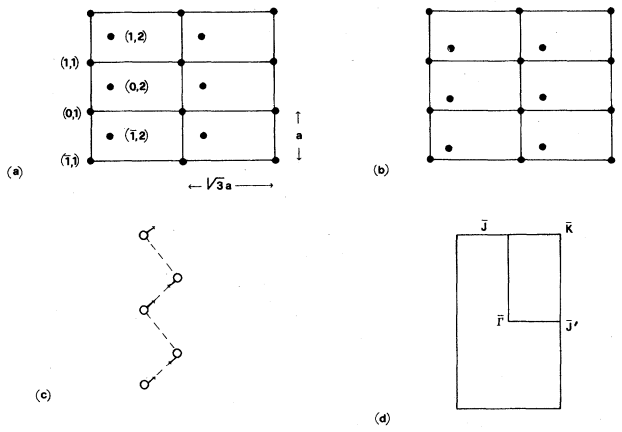

FIG. 7. Atomic arrangement in the surface plane for the π-bonded chain model of Si(111)2×1 (top view): (a) the symmetric chain model, where (n,i) is the ith atom in the nth unit cell, and $a=3.85$ Å; (b) the dimerized chain model (for clarity of the figure, the dimerization is strongly magnified); (c) atomic displacement pattern for the "dimerization mode"; (d) the surface Brillouin zone.

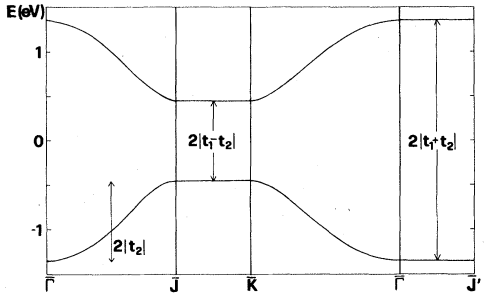

FIG. 8. Surface band structure of the dimerized chain model of Si(111)2×1, with $t_1=-0.9$ eV and $t_2=-0.45$ eV. The zero of the energy scale is the midgap energy, i.e., the surface Fermi level.

so that the surface ground state is, in this case, purely covalent.

To describe the electronic structure of the above model, we assume the one-electron Hamiltonian to be

$$\mathscr{H}=\epsilon\sum_{n,i}|n,i\rangle\langle n,i| + \sum_n t_{1,n}(|n,1\rangle\langle n,2|+|n,2\rangle\langle n,1|) + \sum_n t_{2,n}(|n,1\rangle\langle n-1,2|+|n,2\rangle\langle n+1,1|), \quad (3.1)$$

with $|n,i\rangle$ denoting the ith ($i=1,2$) DB in cell n. Here, ϵ is the DB on-site energy—the same for all DB's—$t_{1,n}$ is the hopping integral between the two DB's connected by the short bond in cell n, and $t_{2,n}$ is the hopping integral between the two DB's connected by a long bond in neighboring cells along a given chain. For uniform dimerization, $t_{1,n}\equiv t_1$ and $t_{2,n}\equiv t_2$, diagonalization of (3.1) yields the DB's dispersion relations:

$$\epsilon_{\pm}(\vec{k})=\epsilon\pm[t_1^2+t_2^2+2t_1t_2\cos(k_y a)]^{1/2}, \quad (3.2)$$

where the minus and plus signs refer to the filled (−) and empty (+) states, respectively. Reasonable values for the band parameters t_1 and t_2 are determined by the following requirements: (a) the valence-band width should be ~0.8 eV, as suggested by angle-resolved photoemission;[40] (b) the optical-absorption peak should occur[2] at ~0.45 eV. In our calculation the absorption spectrum includes both the electron-hole interaction, leading to exciton bound states, and the exciton-lattice coupling, leading to polarons.[41] The exciton-lattice coupling depends strongly on the ratio t_1/t_2, which is related to the magnitude of the ground-state dimerization. Conditions (a) and (b) are well satisfied by taking $t_1=-0.9$ eV and $t_2=-0.45$ eV. The resulting surface band structure is shown in Fig. 8. It does reproduce fairly well the band dispersions resulting from more realistic calculations for this model.[8,19]

We approximate the Wannier functions of our model by simple bonding and antibonding combinations of DB orbitals in the same cell. For negligible overlap between DB's at different sites, we have

$$a_{-n}=\frac{1}{\sqrt{2}}(|n,1\rangle+|n,2\rangle), \quad (3.3)$$

$$a_{+n}=\frac{1}{\sqrt{2}}(|n,1\rangle-|n,2\rangle), \quad (3.4)$$

with energies

$$\epsilon_{\mp n}=\epsilon\pm t_{1,n}. \quad (3.5)$$

For the lower (upper) Wannier state the error involved in this approximation is the neglect of an antibonding (bonding) contribution of amplitude $\alpha\equiv t_2/4t_1\sim 0.12$ from neighboring cells along the chain, more distant cells contributing terms of higher order in α. The Wannier-state energies (3.5), on the other hand, need only corrections of second order in α, which can be neglected.

We shall determine the ground-state configuration and the electron-lattice coupling by assuming that $t_{1,n}$ and $t_{2,n}$ depend on bond lengths according to

$$t_{1,n}=t_0\exp(-\beta\Delta d_{n1}),\quad t_{2,n}=t_0\exp(-\beta\Delta d_{n2}), \quad (3.6)$$

where t_0 is the hopping integral between DB's at distance d_0 (equal to the bulk nearest-neighbor distance $d_b=2.35$ Å), and Δd_{n1} (Δd_{n2}) is the contraction (expansion) of the short (long) bond referred to d_0,

$$\Delta d_{ni}\equiv d_{ni}-d_0. \quad (3.7)$$

The functional form (3.6) has been extensively used in surface electronic-structure calculations to describe the scaling of tight-binding parameters with distance[28] and is quite reasonable as long as $|\Delta d_{ni}|/d_0\ll 1$. The values Δd_{n1} and Δd_{n2} are connected by a simple geometrical relationship in our model. With $d_0=2.35$ Å and $|\Delta d_{ni}|\ll d_0$, bond angles for uniform dimerization are $\theta\sim 109.5°$, resulting in

$$\Delta d_{n2}=-\tfrac{1}{3}\Delta d_{n1}. \quad (3.8)$$

This condition, combined with (3.6) and the values of t_1 and t_2, yields the relation between dimerization parame-

ters and hopping integrals,

$$\beta\Delta d_{n1}=-\tfrac{3}{4}\ln(t_1/t_2)\ , \tag{3.9}$$

numerically, $\beta\Delta d_{n1}=-0.52$. The hopping parameter for the undimerized chains, $t_0=t_1\exp(\beta\Delta d_{n1})$, is then determined to be $t_0=-0.54$ eV in our case. This value is in fair agreement with commonly accepted first-neighbor $(pp\pi)$ interaction parameters in Si.[28]

To calculate the ground-state structural configuration of the surface, we now consider the total energy of our system of $2N$ surface atoms (N is the number of unit cells) and $2N$ electrons occupying lower-band states. Within the Born-Oppenheimer approximation, the total energy is

$$\mathscr{E}_{2N}=\mathscr{E}_{\rm latt}+\mathscr{E}_{\rm el}(\{d_{ni}\})\ , \tag{3.10}$$

where $\mathscr{E}_{\rm latt}$ is the lattice (potential) energy and $\mathscr{E}_{\rm el}(\{d_{ni}\})$ is the electronic energy corresponding to the configuration specified by the d_{ni}'s. To evaluate $\mathscr{E}_{\rm latt}$ we restrict ourselves to the dimerization mode—shown in Fig. 7—and describe it in terms of the force constant γ in the approximate form

$$\mathscr{E}_{\rm latt}=\tfrac{1}{2}\gamma\sum_n[(\Delta d_{n1})^2+(\Delta d_{n2})^2]\ , \tag{3.11}$$

while the electronic energy is simply

$$\mathscr{E}_{\rm el}=2\sum_n\epsilon_{-n}\ , \tag{3.12}$$

with the Wannier-state energies ϵ_{-n} given by (3.5). By minimization, and with the geometrical constraint (3.8), we find

$$\Delta d_{n1}=\tfrac{9}{5}\beta t_1/\gamma\ . \tag{3.13}$$

We need to estimate the values of the parameters β and γ. The dependence of the total energy on bond-length contraction was recently calculated by Pandey[7] for the symmetric chain model of Si(111)2×1. His results—in the form of total energy per surface atom—can be parametrized as follows:

$$\mathscr{E}_{\rm symm}=\text{const}+\tfrac{1}{2}K(\Delta d)^2\ , \tag{3.14}$$

where $K\simeq 18.5$ eV/Å^2 and Δd is the bond-length contraction (expansion) with respect to the calculated equilibrium values, $d_s\simeq 2.2$ Å. Within our scheme, and for small deviations from equilibrium, the total energy per surface atom of the symmetric chain model can be expressed as

$$\mathscr{E}'_{\rm symm}=\text{const}+\tfrac{1}{2}(\gamma+\beta^2t_0)(\Delta d')^2\ , \tag{3.15}$$

where the equilibrium bond-length value—to which $\Delta d'$ is referred—is assumed to be $d_0=2.35$ Å. We ignore the difference between d_s in (3.14) and d_0 in (3.15) and require that our parameter $(\gamma+\beta^2t_0)$ equals the calculated value for K. Combining this condition with (3.9), we obtain $\gamma=22.3$ eV/Å^2 and $\beta=2.7$ Å^{-1}. In the resulting ground-state configuration, bond-length contractions and expansions are then $\Delta d_1^g=-0.194$ Å $\Delta d_2^g=+0.065$ Å. For small displacements, $q_{ni}=\Delta d_{ni}-\Delta d_{ni}^g$, from equilibrium, the total-energy increase, to second order, is

$$\Delta\mathscr{E}=\tfrac{1}{2}\sum_n(\tfrac{10}{9}\gamma+2\beta^2t_1)q_{n1}^2\ . \tag{3.16}$$

This relation defines the frequency ω_0 of the long-wavelength "dimerization mode,"

$$\frac{M}{2}\omega_0^2=\tfrac{10}{9}\gamma+2\beta^2t_1\ , \tag{3.17}$$

yielding $\hbar\omega_0=0.059$ eV with our model parametrization.

B. Electron polaron and hole polaron

We now consider an excess electron which, in the absence of coupling to the lattice, occupies a Bloch state of the conduction band. As discussed in Sec. II B, the localization or delocalization of this excess electron is roughly determined by the ratio E_R^e/B, where E_R^e is the energy released when the lattice relaxes around the localized electron, while B is the kinetic energy of localization of the electron, $B=|t_2|$ in the present model. If $E_R^e>B$, the electron will be localized. Since electrons and holes are perfectly symmetric in this model, we shall restrict our discussion to electrons. Implicitly, all the results will refer also to holes.

We shall also require that the lattice distortions q_{ni} caused by the excess electron satisfy

$$|q_{ni}|\ll|\Delta d_{ni}^g|\ ,$$

where Δd_{ni}^g is the bond-length contraction or dilation in the ground-state dimerized configuration. By this restriction, we shall automatically exclude from our treatment the possibility of soliton formation.

1. *Limit of strongly localized polaron*

We first calculate the relaxation energy assuming that the excess electron is perfectly localized in one cell, say cell 0. We denote by $\{d_{ni}^g\}$ the configuration parameters of the ground state—before the lattice distortion induced by the excess electron—and by $\{d_{ni}^e\}$ those after distortion. Within the adiabatic approximation, the total energy is

$$\mathscr{E}_{2N+1}=\tfrac{1}{2}\gamma\sum_n[(\Delta d_{n1})^2+(\Delta d_{n2})^2]$$
$$+2\sum_n\epsilon_{-n}(d_{n1})+\epsilon_{+0}(d_{01})\ . \tag{3.18}$$

Since we assume perfect localization, the only bond lengths which change after lattice relaxation are $d_{0,1}$, $d_{0,2}$, and $d_{-1,2}$, with

$$\Delta d_{02}=\Delta d_{\bar{1}2}=-\tfrac{1}{6}(\Delta d_{01}+\Delta d_{\bar{1}1})$$

(see Fig. 7). Minimizing $\mathscr{E}_{2N+1}$ with respect to Δd_{01}, we obtain

$$\beta\Delta d_{01}^e\exp(\beta\Delta d_{01}^e)=\tfrac{9}{10}\beta^2t_0/\gamma\ , \tag{3.19}$$

which gives $\Delta d_{01}^e=-0.069$ Å and $\Delta d_{02}^e=\Delta d_{\bar{1}2}^e=+0.044$ Å. As shown by Fig. 9(a) the lattice distortion caused by the excess electron is a local reduction of the dimerization with respect to the ground-state configuration.

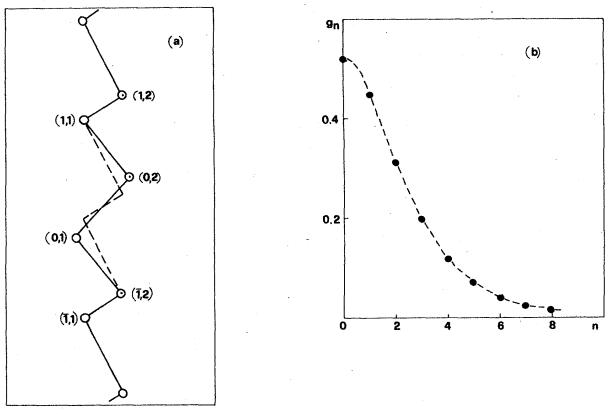

FIG. 9. (a) Qualitative picture of the lattice distortions caused by a strongly localized excess electron for the dimerized chain model. (b) Electron-polaron envelope function g_n, Eq. (3.27); n is the cell label along a given chain; g_n is symmetric for $n \to -n$.

This, in turn, implies a reduction of the lattice potential energy and, correspondingly, an increase of the lower-band-electron energy, since the bonding energy $|t_{10}^e|$ is decreased. Overall, the relaxation energy is

$$E_R^e \equiv \mathscr{E}_{2N+1}(\{d_{ni}^g\}) - \mathscr{E}_{2N+1}(\{d_{ni}^e\}) = 0.14 \text{ eV} .$$

This value must be compared with $B=0.45$ eV for the kinetic energy of localization. Since here $E_R^e \ll B$, we deduce that, unlike in the buckling model of Sec. II, in this case the excess electron will not stay localized, but will spread to find a configuration energetically more favorable. This is substantially confirmed by the value of the Huang-Rhys factor S^e. The expression for S^e at $T=0$ K is $S^e = E_R^e/\hbar\bar{\omega}_0$,[26,27] where $\bar{\omega}_0$ is an appropriate average between ω_0^g, the phonon frequency in the ground state, defined by (3.17), and ω_0^e, the local value of the phonon frequency in the presence of the excess electron. The local frequency is

$$\omega_0^e = \left[\frac{2}{M} \left(\tfrac{10}{9}\gamma + \beta^2 t_1^e \right) \right]^{1/2} .$$

Numerically, $\hbar\omega_0^e = 0.077$ eV, resulting in $S^e \sim 2.1$, a value which indicates an intermediate-coupling situation [the mass enhancement is $\exp(S_e) \sim 8$]. Note that ω_0^e is larger than the phonon frequency in the ground state.

2. *Polaron radius*

To account for the spatial extent of the polaron, we now express the wave function of the excess electron as a linear combination of upper Wannier states $|n_+\rangle$,

$$\psi_e = \sum_n c_n |n_+\rangle , \tag{3.20}$$

with coefficients c_n normalized to unity, $\sum_n |c_n|^2 = 1$. For

$$\Psi = \psi_e \chi_{\text{vib}} \prod_n |n_-\rangle ,$$

the total-energy expectation value $\langle \Psi | H | \Psi \rangle$ is

$$\mathscr{E}_{2N+1} = \tfrac{1}{2}\gamma \sum_n [(\Delta d_{n1})^2 + (\Delta d_{n2})^2] + 2\sum_n (\epsilon + t_{1,n}) + \sum_n (\epsilon - t_{1,n}) |c_n|^2 + \sum_n t_n (c_n^* c_{n+1} + c_n^* c_{n-1}) , \tag{3.21}$$

where $t_n \equiv -\frac{1}{2}t_{2,n}$ is the hopping integral between $|n_+\rangle$ and $|(n\pm1)_+\rangle$. Since we assume that the distortion of the ground-state configuration is small, i.e.,

$$\Delta d_{ni}^e = \Delta d_{ni}^g + q_{ni} \quad \text{with} \quad |q_{ni}/\Delta d_{ni}^g| \ll 1 ,$$

we can use

$$t_{1,n} = t_1(1 - \beta q_{n1}) , \tag{3.22}$$

where $|t_1|$ is the value of the bonding energy in the ground state. For simplicity, we shall neglect the dependence of t_n on the cell index by taking $t_n \equiv -\frac{1}{2}t_2$. Since the present situation is of intermediate-coupling type, we are in the embarrassing situation that neither the strong-coupling approximations nor the weak-coupling ones are really quantitatively reliable. Another way of saying this, is that, in principle, we are not allowed any kind of adiabatic approximations, such as (a) freezing the Δd_{ni}, determining the corresponding c_n, and, by substitution into (3.21), obtaining the adiabatic potential $\mathscr{E}_{2N+1}$ as a functional of Δd_{ni} alone (good for strong coupling), or (b) freezing the c_n, determining the corresponding Δd_{ni}, and, by substitution into the minimum condition of (3.21), with respect to c_n, obtaining an equation for c_n alone (good for weak coupling). Rather than going into more elaborate intermediate-coupling methods,[32] we have chosen to follow route (b) anyway, because it is still qualitatively correct, if numerically inaccurate, and also because it has, in this case, less variational parameters to be determined than the corresponding SC treatment. Freezing the electronic coefficients c_n first, the minimum condition with respect to the lattice coordinates yields

$$q_{n1} = -\frac{1}{2} \frac{\Delta d_1^g}{1 + \beta \Delta d_1^g} |c_n|^2 , \tag{3.23}$$

i.e., the excess electron acts to reduce the dimerization magnitude. Substituting into (3.21) we obtain, to first order in q_{n1},

$$\mathscr{E}_{2N+1} = \text{const} + \tfrac{10}{9}\gamma \, \Delta d_1^g \sum_n q_{n1} - 2\beta t_1 \sum_n q_{n1} + \sum_n (\epsilon - t_1 + \beta t_1 q_{n1}) |c_n|^2 - \tfrac{1}{2} t_2 \sum_n (c_n^* c_{n+1} + c_n^* c_{n-1}) .$$

By virtue of (3.23), the second and third terms correspond to the elastic gain obtained by "undimerization" and to the related electronic loss in the filled lower band. Using (3.13), we see that these two terms cancel exactly in this case,[42] leaving

$$\mathscr{E}_{2N+1}=\text{const}+\sum_n(\epsilon-t_1+\beta t_1 q_{n1})\,|\,c_n\,|^2$$
$$-\tfrac{1}{2}t_2\sum_n(c_n^*c_{n+1}+c_n^*c_{n-1})\ .$$

We can therefore focus on the motion of the excess electron—the distortion being caused by the electron itself through (3.23)—and ignore from now on the valence electrons. Our treatment now follows closely that of Holstein.[43]

The coefficients c_n of the electron wave function satisfy the Euler equation generated by the above form of $\mathscr{E}_{2N+1}$,

$$(\epsilon-t_{1,n})c_n-\tfrac{1}{2}t_2(c_{n+1}+c_{n-1})=Ec_n\ ,$$

where E is the polaron energy. We use (3.22) and (3.23) to relate $t_{1,n}$ to $|\,c_n\,|^2$ self-consistently,

$$t_{1,n}=t_1+A\,|\,c_n\,|^2,\quad A\equiv\frac{1}{2}\frac{\beta\Delta d_1^{\xi}}{1+\beta\Delta d_1^{\xi}}\ ,\quad t_1>0\ . \tag{3.24}$$

We then obtain

$$(\epsilon_p-A\,|\,c_n\,|^2)c_n-\tfrac{1}{2}t_2(c_{n+1}+c_{n-1}+2c_n)=0\ , \tag{3.25}$$

where $\epsilon_p=(\epsilon-t_1+t_2)-E$ is the polaron binding energy referred to the bottom of the upper band at J, $\epsilon_+(J)=\epsilon-t_1+t_2$. Equation (3.25) can be solved by taking $c_n=(-1)^n g_n$ and using the continuum approximation,

$$g_{n+1}+g_{n-1}-2g_n\sim\frac{d^2g_n}{dn^2}\ .$$

The bound-state solutions ($\epsilon_p>0$) have the form[43]

$$g(n-n_0)=\left[\frac{2\epsilon_p}{A}\right]^{1/2}\operatorname{sech}\left[\left[\frac{2\epsilon_p}{|\,t_2\,|}\right]^{1/2}(n-n_0)\right]\ , \tag{3.26}$$

where the cell index n_0 labels the (infinitely degenerate) set of localized solutions,

$$\psi_e(n_0)=\sum_n(-1)^n g(n-n_0)\,|\,n_+\,\rangle\ , \tag{3.27}$$

analogous of the upper Wannier states for the problem without coupling. The polaron binding energy can be determined using the normalization constraint $\int dn\,g^2(n)=1$, which yields

$$\epsilon_p=\frac{A^2}{8\,|\,t_2\,|}\ . \tag{3.28}$$

Using $A=0.49$ eV, as given by (3.24), we find $\epsilon_p=0.066$ eV. The polaron radius

$$r_p^e=\left[\frac{|\,t_2\,|}{2\epsilon_p}\right]^{1/2} \tag{3.29}$$

is then of the order of 7 Å (approximately two surface cells), confirming the intermediate-coupling nature discussed earlier. The envelope function (3.26) is shown in Fig. 9(b).

3. Polaron bands

The localized states (3.27) are not yet complete solutions of the polaron problem. Because of the translational symmetry, the true polaron eigenstates should be Bloch functions labeled by $\vec{k}$, the total momentum of the electron and phonon system

$$\Psi_{\vec{k}}=N^{-1/2}\sum_{n_0}e^{ikn_0}\psi_e(n_0)\chi(n_0)\ ,$$

where $\chi(n_0)$ is the vibrational wave function of the lattice when the electron is in the state $\psi_e(n_0)$. The eigenvalues corresponding to Ψ_k then form a band whose width is substantially reduced with respect to the bare width $2B=2\,|\,t_2\,|$, since hopping integrals are multiplied by the overlap between the lattice wave functions. One way to determine the polaron band energy is, of course, to just evaluate the expectation value

$$E_k=\langle\Psi_k\,|\,H\,|\,\Psi_k\rangle/\langle\Psi_k\,|\,\Psi_k\rangle\ .$$

However, we prefer to calculate the polaron band dispersion in a different (though, in principle, equivalent) way. Using Bloch eigenstates to represent the excess electron wave function, we determine the polaron energies E_k by solving the Dyson equation[26,44]

$$E_k=\epsilon_+(k)+\Delta_k(E_k)\ , \tag{3.30}$$

where $\Delta_k(E_k)$ is the real part of the electron self-energy, after averaging over the state of the phonon system (at thermal equilibrium). While this procedure is not really more convenient than calculating $\langle\Psi_k\,|\,H\,|\,\Psi_k\rangle$ in this case, having established it it will be very convenient later, for the problem of the electron-hole polaron.

We set our total Hamiltonian $\mathscr{H}_{\text{tot}}$ as the sum

$$\mathscr{H}_{\text{tot}}=\mathscr{H}_e+\mathscr{H}_L+\mathscr{H}'\ , \tag{3.31}$$

consisting of an electronic part,

$$\mathscr{H}_e=\sum_{\vec{k}}\epsilon_+(\vec{k})c_{\vec{k}}^{\dagger}c_{\vec{k}}\ , \tag{3.32}$$

of a lattice contribution

$$\mathscr{H}_L=\hbar\omega_0\sum_{\vec{k}}b_{\vec{k}}^{\dagger}b_{\vec{k}}\ ,$$

and of a coupling term,

$$\mathscr{H}'=\sum_{\vec{k},\vec{k}'}V_{\vec{k}\vec{k}'}(b_{-\vec{k}+\vec{k}'}^{\dagger}+b_{\vec{k}-\vec{k}'})c_{\vec{k}}^{\dagger}c_{\vec{k}'}\ . \tag{3.33}$$

In (3.32), $c_{\vec{k}}^{\dagger}$ creates a Bloch electron in the upper band, and $\epsilon_+(\vec{k})$ is the corresponding energy, the lattice being frozen in its ground-state configuration. Since we are interested in states close to the band edge along the $\bar{\Gamma}\bar{J}$ direction (see Fig. 7), we shall use the simplified dispersion $\epsilon_+(k)=\hbar^2k^2/2m_e^*$, k being measured relative to the $\bar{J}$ point. We take the effective mass m_e^* to be $0.57m_0$, as required by our band structure (3.2). In the lattice Hamiltonian H_L, we have restricted our attention to the optical mode modulating the dimerization along the chains, which is taken to be Einstein-like, $\omega_k\equiv\omega_0$, with ω_0 given

by (3.17). Finally, $V_{\vec{k}\,\vec{k}}$, is evaluated as a function of the derivative of the band energy at $k=0$ (point $\bar{J}$ of the SBZ), with respect to the lattice displacements, in the following way.[45]

Let us call $\hat{\phi}(n)$ the dimerization amplitude operator in cell n,

$$\hat{\phi}(n)=\sum_{\vec{q}} u_{\vec{q}}(b^{\dagger}_{\vec{q}} e^{i\vec{q}\cdot\vec{R}_n}+\text{H.c.}) , \tag{3.34}$$

where $u_q=u_{1q}-u_{2q}$ and u_{1q},u_{2q} are the displacement amplitudes of atoms 1 and 2 in the chain. In the simplest model of a diatomic chain, we have

$$u_q=\left[\frac{\hbar}{M\omega_0}\right]^{1/2}+O(q^2) .$$

If we call

$$D=\frac{d\epsilon_+(k=0)}{d\hat{\phi}}L$$

the deformation potential, where L is the bond length, the coupling $V_{kk'}$ is obtained as

$$V_{kk'}=D\left\langle k\left|\frac{d\hat{\phi}}{dR_n}\right|k'\right\rangle$$

$$=iD(k-k')u_{k-k'} . \tag{3.35}$$

For our purposes, the presence of the k-dependent interaction $V_{kk'}$ in this formula is rather inconvenient, turning the self-energy calculation into a somewhat extensive numerical problem. For the sake of simplicity, we then replace the true expression (3.35) with a crudely approximate k-independent value,

$$V_0=Du_0/L . \tag{3.36}$$

The deformation potential is easily derived from the tight-binding energy to be

$$D=-\beta L\,|\,t_1+\tfrac{1}{3}t_2\,| .$$

With our parameter values, $u_0=(\hbar/M\omega_0)^{1/2}=0.095$ a.u., $L=4.44$ a.u., and $D=6.6$ eV, this yields $V_0=0.14$ eV. We stress that in view of the large arbitrariness involved in the approximation of replacing $V_{\vec{k}\,\vec{k}}$, by V_0, our numerical results will have only order-of-magnitude significance.

Our electron self-energy $\Sigma_k(E)$ satisfies the approximate Brillouin-Wigner equation[26]

$$\Sigma_k(E)=\sum_{k'}|V_{kk'}|^2\left[\frac{n(\omega_{k-k'})+1}{E-\epsilon_{k'}-\hbar\omega_{k-k'}-\Sigma_{k'}(E-\hbar\omega_{k-k'})}+\frac{n(\omega_{k'-k})}{E-\epsilon_{k'}+\hbar\omega_{k'-k}-\Sigma_{k'}(E+\hbar\omega_{k'-k})}\right] , \tag{3.37}$$

where $n(\omega_k)$ is the phonon thermal-occupation number. It is easy to verify that with our approximations, $\omega_k\equiv\omega_0$ and $V_{kk'}\equiv V_0$; $\Sigma_k(E)$ is also independent of k. This allows the explicit evaluation of the sum over k' in (3.37), which, of course, simplifies a great deal the numerical iterative solution of $\Sigma(E)$. The details of this calculation are given in Appendix B. The resulting real and imaginary parts of (3.37), $\Delta(E)$ and $\Gamma(E)$, are plotted in Fig. 10 for $T=0$ and 300 K. At $T=0$ K the dominant feature of $\Delta(E)$ is the inverse-square-root singularity—related to the one dimensionality of this model—occurring at an energy E^* slightly above the unperturbed band edge (the zero of our energy scale). At the same energy E^*, $\Gamma(E)$ (which is zero below E^*) also has an inverse-square-root singularity, and is then finite and positive at higher energies. In Fig. 10 we also show the graphical solution of the Dyson equation (3.30) for a few values of the electron bare energy $\epsilon_+(k)$. The $k=0$ ($\bar{J}$ point) renormalized electron energy $E_0=\Delta(E_0)$ is -0.051 eV, which yields a polaron radius, $r_p^e\sim(2m_e^*\,|E_0|/\hbar^2)^{-1/2}$, of the order of three unit cells, in substantial agreement with the results of the preceding subsection. The energy E^* defined above is simply $E^*=E_0+\hbar\omega_0$. Because of the singular behavior of $\Delta(E)$, it is always possible to find a solution of (3.30) in the range $(E_0, E_0+\hbar\omega_0)$, for any value of the bare energy $\epsilon_+(k)$. The free-electron parabola $\epsilon_+(k)=\hbar^2k^2/2m_e^*$ is modified into (a) a lower band compressed between E_0 and $E_0+\hbar\omega_0$, and (b) an upper band which exists only for $k>(2m_e^*E^*/\hbar)^{1/2}$ and tends asymptotically to $\hbar^2k^2/2m_e^*$ for large k. The $T=0$ K "polaron band structure" is shown in Fig. 11, where both bands—when coexisting—are indicated. Noting that our starting problem has full electron-hole symmetry, all results derived above for electrons also remain valid for holes, once the sign of all energies is reversed.

At $T\neq0$ K, phonon absorption processes also contribute to $\Sigma(E)$, as shown by (3.37). The calculated real and imaginary parts of $\Sigma(E)$ at $T=300$°K are shown in Fig.

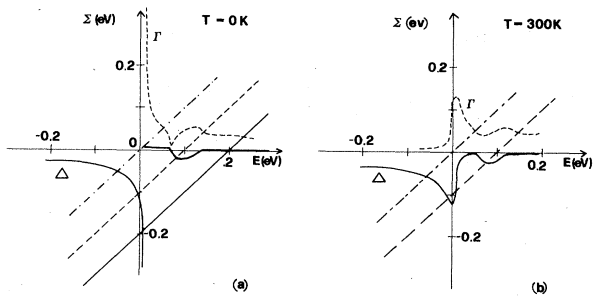

FIG. 10. Real (Δ) and imaginary (Γ) parts of the electron and hole self-energies, Eq. (3.37): (a) at $T=0$ K and (b) at $T=300$ K. The zero of the energy scale here is the bottom of the conduction band at $\bar{J}$ (on top of the valence band for the hole). The intersections between the lines $E-\epsilon^0(k)$ and $\Delta(E)$ give the solutions of the Dyson equation (3.30).

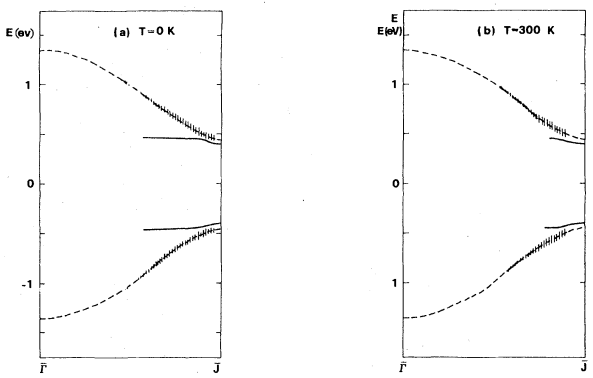

FIG. 11. Polaron bands along the chain direction $\bar{\Gamma}\bar{J}$, obtained by solution of the Dyson equation as shown in Fig. 10: (a) at $T=0$ and (b) at $T=300$ K. The dashed lines are the bare bands, before coupling to the lattice. The solid lines show the first, sharp polaron band. The hatched area is centered about the midpoint of the second, broad polaron band, its width reflecting the corresponding energy width 2Γ.

10(b). At finite T, all singularities are smoothed out because of the finite value of Γ throughout the spectrum. A cutoff wave vector appears, whereby the lower branch of polaron states remains well defined only out to a certain value, as illustrated by the graphical solution of the Dyson equation in Fig. 10(b). This cutoff wave vector is as small as ~ 0.15 Å^{-1} at $T=300$ K, while the shift increases gently from 51 to ~ 60 meV.

C. Excitons

As a preliminary step for the calculation of the optical spectrum, in this subsection we study surface-state excitons, particularly, singlets of total momentum $\vec{k}=\vec{0}$. We shall be interested in the way such excitons are affected by coupling to the surface lattice. To this end we must, however, first study excitons in a frozen lattice. To simplify matters, we shall assume the electron and the hole to be on the same chain. One further motivation for this assumption is that the optical cross section for creation of electron-hole pairs on different chains is exponentially small due to the large interchain separation.

Using a standard approach,[21] we expand the exciton wave function in terms of singlet states $\psi(k_e,k_h)$ with an electron in the upper Bloch state k_e and a hole in the lower state k_h,

$$\Phi(k=0)=\sum_{k'} c(k')\psi(k',k') . \tag{3.38}$$

The coefficients $c(k)$ obey the equation

$$\sum_{k'}\{[\epsilon_+(k)-\epsilon_-(k)-E_B]\delta_{kk'}+W(k,k')\}c(k')=0 , \tag{3.39}$$

where E_B is the exciton binding energy and $W(k,k')$ is the sum of the electron-hole exchange and Coulomb interaction potentials. For vanishing overlap between Wannier functions of different cells, $W(k,k')$ can be expressed as

$$W(k,k')=N^{-1}\sum_{\vec{l}} e^{i(\vec{k}-\vec{k}')\cdot\vec{l}} w(\vec{l}) , \tag{3.40}$$

with

$$w(\vec{l})=\begin{cases} 2\sum_{\vec{m}} X(\vec{m})-C(0), & \vec{l}=\vec{0} \\ -C(\vec{l}), & \vec{l}\neq\vec{0} . \end{cases}$$

Here,

$$X(\vec{l})=\int d^3r\, d^3r'\, a^*_{+0}(\vec{r})a_{-0}(\vec{r}) \times\frac{e^2}{\epsilon_{bg}|\vec{r}-\vec{r}'|}a^*_{-l}(\vec{r}')a_{+l}(\vec{r}') \tag{3.41}$$

is the exchange interaction between electron and hole separated by $\vec{l}$, while

$$C(\vec{l})=\int d^3r\, d^3r'\,|a_{+l}(\vec{r})|^2\frac{e^2}{\epsilon_s|\vec{r}-\vec{r}'|}|a_{-0}(\vec{r}')|^2 \tag{3.42}$$

is the corresponding electron-hole Coulomb interaction. In (3.41), $\epsilon_{bg}\sim(\epsilon_b+1)/2$ is the background screening accounting for bulk polarization effects not directly included in our treatment, while ϵ_s in (3.42) should also include the screening of DB electrons, $\epsilon_s=\epsilon_{bg}+(\epsilon_{DB}-1)$.[35] The DB screening is known to be ineffective (i.e., $\epsilon_{DB}=1$) at short and long distances,[46] but can be significant at intermediate distances, where virtual transitions between DB's can occur.

In order to calculate $X(\vec{l})$ and $C(\vec{l})$, we expand the Wannier functions into DB orbitals, retain only two-center integral terms, and evaluate the Coulomb interaction between charge distributions centered at different sites with the point-charge approximation, similar to what was done in Sec. II C for the buckling model. With the above simplifications the central-cell potential $W(0)$ becomes

$$W(0)=\tfrac{1}{2}U-E_M-\tfrac{1}{2}V_c(|R_{01}-R_{02}|) , \tag{3.43}$$

where U is the intrasite repulsion, $V_c(R)\equiv e^2/\epsilon_s R$, and E_M is a lattice sum of dipole-dipole—type interactions,

$$E_M=V_x(|\vec{R}_{01}-\vec{R}_{02}|) + \sum_{m'(\neq 0)}[V_x(|\vec{R}_{01}-\vec{R}_{m'2}|)-V_x(|\vec{R}_{01}-\vec{R}_{m'1}|)] ,$$

with $V_x(R)\equiv e^2/\epsilon_{bg}R$.

We take $U=1.9$ eV, as for the buckling model; the calculated value of E_M is 0.62 eV, including both intrachain and interchain contributions. We approximate the surface screening function ϵ_s at distances of first, second, and third neighbors using the expression suggested by Keldysh[47,48] and based on the macroscopic three-layer model. In our case, we find $\epsilon_s=15.3$, 12.8, and 9.6 for first, second, and third neighbors, respectively. The resulting exciton potential $W(\vec{l})$ along the chain is shown in Fig. 12(a).

We calculate the exciton binding energy E_B by direct

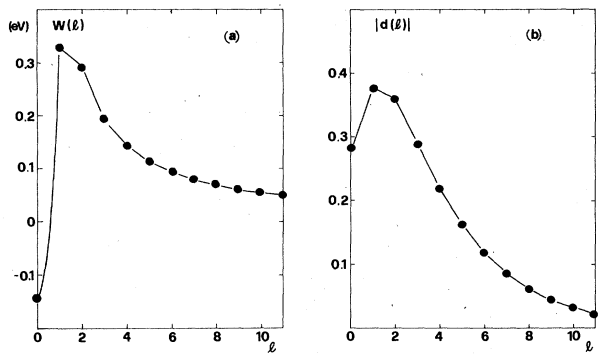

FIG. 12. (a) Electron-hole—interaction potential (inverted) for singlet excitons along the chain direction using $U=1.9$ eV, $\epsilon_{bg}=6.5$, and DB screening evaluated according to the macroscopic three-layer model (see text). (b) Envelope function for the lowest singlet exciton.

diagonalization of (3.39) over a suitable mesh of $\vec{k}$ points along the $\bar{\Gamma}\bar{J}$ direction of the SBZ. The resulting value of E_B is 0.20 eV, of the same order as other independent estimates for surface-state excitons.[23,48] In Fig. 12(b) we show the exciton envelope function in real space,

$$d(\vec{l})=N^{-1/2}\sum_k c(k)e^{i\vec{k}\cdot\vec{l}} ,$$

representing the probability amplitude for the electron and hole to be at distance $\vec{l}$. Our exciton is mostly localized on nearest- and next-nearest-neighbor cells with an average radius $r_{exc}\sim 4$ unit cells.

The next higher (singlet) exciton state is found at an energy 0.86 eV, i.e., 0.16 eV above the lowest singlet and just 4 meV below the upper surface band edge, and is totally insensitive to the details of the central-cell potential (e.g., the value of U), as it is appropriate to large-radius excitons. In contrast, the energy of the optically inactive *triplet* exciton [which can be calculated in the same way as the lowest singlet exciton, but excluding the exchange potential from (3.39)] is strongly dependent on the details of the potential in the central cell; in particular, large values of U would tend to give a *negative* triplet excitation energy, thus implying an instability of the ground state against triplet-exciton formation (i.e., antiferromagnetism).[49] With our parameters values, the triplet binding energy is ~ 0.6 eV, resulting in a positive excitation energy ~ 0.3 eV from the ground state. Interestingly, triplet excitons also play an important role on the buckled surface models. Del Sole and Chadi,[13] in particular, noted that with large but not unrealistic Hubbard U's, the buckled surface was also unstable against formation of triplets, thus turning into a two-dimensional antiferromagnet.

D. Excitonic polaron

The coupling of the exciton to the lattice in our model is characterized by the polaron radii for the single (unbound) electron and hole being of the same order of the exciton radius in the frozen lattice (see Secs. III B and III C). In such cases a strong interference between the electron-hole and the electron-lattice interactions can occur, so that the two terms should be treated simultaneously.[23–25] A similar situation occurred for the buckling model, and actually the electron-hole and electron-lattice couplings were both included in the minimization of the total adiabatic energy (see Sec. II D). The approach used for that case, however, is not convenient for the chain model, essentially because the exciton and polaron states extend over a large number of unit cells. For this reason we use a $\vec{k}$-space formulation consistent with the preceding part of this section.

We proceed as in Sec. III B 1, replacing the electron Bloch states by exciton states $|k\rangle$, where k denotes the total momentum.[26] We consider only the lowest (singlet) exciton, since the energy separation of the next-excited state as well as of the continuum is rather large compared to the phonon frequency. We describe the exciton propagation along the chain by the effective-mass dispersion

$$\epsilon_k^{exc}=\epsilon_0^{exc}+\frac{\hbar^2k^2}{2m_{exc}^*} , \tag{3.44}$$

where $\epsilon_0^{exc}\equiv E_g-E_B$ ($=0.7$ eV with $E_g=0.9$ eV and $E_B=0.2$ eV) is the exciton energy in the frozen lattice, $m_{exc}^*=m_e^*+m_h^*$ ($\sim 1.14m_0$) is the exciton mass, and k is the total momentum in the chain direction, measured relative to the $\bar{J}$ point where the minimum gap occurs. The exciton Hamiltonian—corresponding to (3.32) in Sec. III B—is then

$$\mathscr{H}_{exc}=\sum_k \epsilon_k^{exc}|k\rangle\langle k| . \tag{3.45}$$

The lattice Hamiltonian $\mathscr{H}_L$ is the same as in Sec. III B, Eq. (3.33). The coupling of the exciton to the optical dimerization mode is included by adding a term of the form

$$\mathscr{H}'=\sum_{k,k'} V_{kk'}(b^\dagger_{-k+k'}+b_{k-k'})|k\rangle\langle k'| . \tag{3.46}$$

Once again, we approximate the matrix element $V_{kk'}$ by a constant $V_{exc}\equiv V_{00}\equiv(\hbar/M\omega_0)^{1/2}\Lambda$, where Λ is the derivative of the exciton energy (at $k=0$) with respect to the dimerization amplitude. A simple estimate for Λ which neglects the dependence of the exciton binding energy on atomic displacements is

$$\Lambda=\frac{dE_g}{dq_1}=2\frac{d|t_1-t_2|}{dq_1} , \tag{3.47}$$

where q_1 is the length variation of the short bond, while the stretched bond has $q_2=-\frac{1}{3}q_1$ according to the constraint (3.8). With this approximation, $V_{exc}=2V_0$ ($=0.28$ eV), where V_0 is the coupling constant (3.36) for a single electron or hole, and correspondingly the exciton-polaron shift Δ_{exc} is about 4 times the shift for the electron-polaron or hole-polaron shifts [using (3.37), we find $\Delta_{exc}=-0.21$ eV at $T=0$ K]. We expect this value to be an overestimate, since the choice (3.47) implicitly assumes a complete overlap between the lattice distortions induced by the electron and the hole separately. A correct estimate should probably be intermediate between our value and that for a large-radius exciton (i.e., $r_{exc}\gg r_p^e, r_p^h$), for which the polaron shift is just the sum

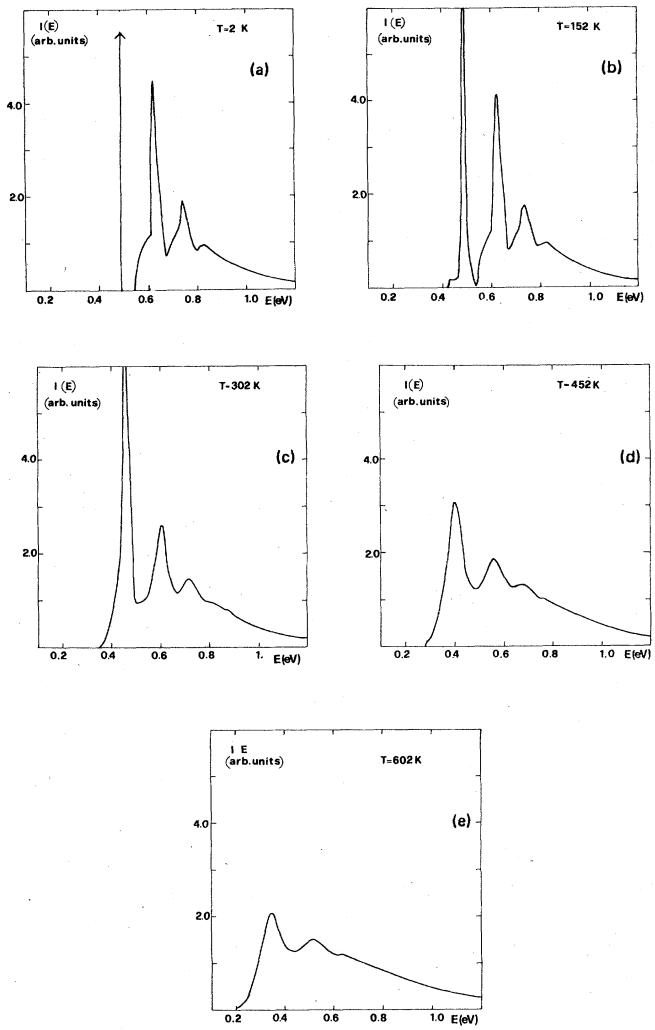

FIG. 13. Absorption spectrum of the dimerized chain model at various temperatures calculated according to (3.48). Note that before these calculated line shapes can be compared with experiment, the additional rigid blue shift discussed in Sec. IV A must be considered. The origin of the oscillations is described in the text.

of the shifts for the single (unbound) electron and hole[32] (in that limit, $\Delta_{\rm exc}\sim -0.1$ eV for our model).

E. Absorption line shape of the π-bonded dimerized chain model

The absorption line shape is strongly dependent on whether the exciton is in a "free" (weak-coupling) or self-trapped (strong-coupling) state. Toyozawa's[26] criterion for exciton self-trapping is $V_{\rm exc}\gg B_{\rm exc}$, where $V_{\rm exc}$ is the coupling constant defined in Sec. III D, and $B_{\rm exc}$ is the exciton effective bandwidth. In our case, a fair estimate for $B_{\rm exc}$ is $B_{\rm exc}\sim\frac{1}{2}|t_2|$ ($\sim$0.23 eV), since $|t_2|$ is the half width of both the hole and the electron bands. This yields $V_{\rm exc}/B_{\rm exc}\sim 1$, characterizing an intermediate-coupling situation. Accordingly, the absorption spectrum is expected to be more complicated than for the limiting situations of WC (Lorentzian line shape) or SC (Gaussian line shape). To calculate the line shape, we use

$$I(E)=\frac{I_0}{\pi}\frac{\Gamma_{\rm exc}(E)}{[E-\epsilon_0^{\rm exc}-\Delta_{\rm exc}(E)]^2+\Gamma_{\rm exc}^2(E)}\ , \qquad (3.48)$$

where $\Delta_{\rm exc}(E)$ and $\Gamma_{\rm exc}(E)$ are the real and imaginary parts of the exciton self-energy calculated using (3.37). Self-consistency modifies the simple Lorentzian shape predicted by lowest-order (Rayleigh-Schrödinger) perturbation theory (good for the extreme WC), giving rise to multiple-phonon structures which can be interpreted as indirect transitions involving phonon emission and/or absorption. Our calculated absorption spectra at various temperatures are shown in Fig. 13. The overall shape of the spectra retains the typical one-dimensional character appropriate to our model. It is interesting to note that the energy separation between the various phonon structures approximately corresponds to twice the phonon frequency. The reason why these structures appear is because the transition probability to exciton states of total momentum $k\cong 0$—involving an even number of phonons in our model—is very high, because the density of states of a one-dimensional band is divergent at the edges. The effect of increasing temperature is a broadening and smoothing out of the structures of the spectra, as usual, as well as causing shifts towards lower frequencies. The position of the first peak—which should be identified with the peak observed experimentally in Ref. 2, is given at various temperatures in Table II.

TABLE II. Position and half width $\Gamma_0\equiv\Gamma(E_0)$ of the main peak in the absorption spectrum of the dimerized chain model of Si(111)2×1 as a function of temperature, as given by Eq. (3.37). In the absence of coupling to the lattice, the peak position would be $\epsilon_0=0.70$ eV. Note that the values of E_0 in this table do not include the effect of the temperature dependence of the reconstruction magnitude discussed in Sec. IV A. This additional effect is included in the values reported in Table III.

T (K)	E_0 (eV)	Γ_0 (eV)
2	0.49	1.5×10^{-5}
152	0.49	9.1×10^{-3}
302	0.45	4.4×10^{-2}
452	0.40	8.8×10^{-2}
602	0.35	0.13

IV. EXPERIMENTAL CONSEQUENCES OF THE EXISTENCE OF SURFACE-STATE POLARONS

This section deals with experimental consequences of the existence of surface-state polarons, as exemplified by the models studied in the preceding sections. Here we will discuss two classes of effects. The first class consists of effects on optical absorption and luminescence from surface states. The theory of these optical processes in the presence of polaron effects is long understood, and through it we can make, particularly for absorption, detailed predictions on line shape and its temperature depen-

dence. The effects in the second class are new and constitute a rather more speculative part of this paper. They concern (a) spectroscopic effects that might become visible in angle-resolved surface photoemission near E_F and in the new technique of scanning tunneling spectroscopy of Binnig and Röhrer,[50] and (b) possible Wigner crystallization of surface-state polarons on heavily doped semiconductor surfaces. A quantitative theory of these effects has not yet been worked out at this stage, and we plan to devote some work to it in the future. Nevertheless, it seems of use to present here a first qualitative discussion of these potentially interesting situations.

A. Temperature-dependent optical absorption; strong coupling versus weak coupling

The optical-absorption calculation for the strong-coupling Si(111)2×1 buckling model was outlined earlier in Sec. II. A weak-coupling calculation of the optical absorption of Si(111)2×1 in the π-bonded chain model is correspondingly given in Sec. III.

For strong coupling, the absorption line shapes are Poisson-like in shape, as in colour centers,[27] as exemplified by Fig. 6. The fine-structure oscillations in this figure are due to our assumption of narrow δ-function-like phonon lines, and may or may not in reality be washed out by finite phonon lifetimes. With increasing T, the peak position approaches more and more closely to the Franck-Condon limit for a "vertical" transition in a configuration-coordinate picture such as that in Fig. 5. As in F-center absorption,[27] this implies a weak to negligible blue shift with increasing T, associated with a linewidth increasing asymptotically like $\sqrt{T}$. For the actual parameters describing our model of the buckled Si(111)2×1 surface, this temperature-dependent shift turns out to be essentially insignificant, as shown by Fig. 6.

In the alternative case of intermediate-coupled π-bonded chains, the optical-absorption mechanism is more closely related to that of bulk Si: transitions occur between the ground state and a fully relaxed excited state. The peak position should shift towards the red, for increasing T, as in bulk Si, due chiefly to the usual Fan[51] mechanism of increasing self-energy with T. This absorption line is (motionally) narrow,[26] and all line-shape effects are due to the electronic band dispersion, which is strong in this case.

This contrasting temperature behavior of the strong- and weak-coupling models is worth considering in more detail as it may provide a useful clue towards identifying the actual reconstruction mechanism of Si(111).

In addition to the "intrinsic" shifts discussed above—a weak or negligible blue shift for buckling, or a Fan red shift for π-bonded chains—we must consider the concomitant effect of a generally temperature-dependent magnitude of the reconstruction itself. This is the equivalent of lattice expansion in a bulk problem. The $T=0$ K reconstruction magnitudes $\phi(0)$ and $\phi(0)=H_1^g-H_2^g$ for buckling, and $\phi(0)=-\Delta d_{1g}$ for the dimerized π-bonded chain, are such as to minimize the total energy $E_{\rm tot}$ at $T=0$ K. However, as T increases, the corresponding minimum of the total free energy $F_{\rm tot}$ will, in general, be attained at different effective reconstruction magnitudes, i.e.,

$$\phi(T)=H_1(T)-H_2(T) \tag{4.1a}$$

for buckling, or

$$\phi(T)=-\Delta d_1(T) \tag{4.1b}$$

for a π-bonded chain. The state favored at high T is one that is "softer," both electronically and vibrationally, and thus has a larger entropy (like an expanded crystal in a bulk case).[52] The free energy depends on the effective magnitude ϕ of the reconstruction in a way that can be generally written as an expansion,

$$F_{\rm tot}=F_0+c(\Delta\phi)^2+f(\Delta\phi)^3+\cdots , \tag{4.2}$$

where $\Delta\phi(T)\equiv\phi(T)-\phi(0)$. The presence of the anharmonic coefficient f implies that the distortion will vary with increasing T, roughly in the form described by Kittel,[53]

$$\Delta\phi(T)=-\frac{3f}{4c^2}k_BT . \tag{4.3}$$

For the case of buckling, we obtain, from (2.12), at $T=0$ K,

$$\begin{aligned} c_b&=\frac{1}{4}\left[\gamma-\frac{C}{a^2}-\frac{64t^2a^2}{C(H_1^g+H_2^g)(H_1^g-H_2^g)^3}\right] , \\ f_b&=\frac{16t^2a^2}{C(H_1^g+H_2^g)(H_1^g-H_2^g)^4} . \end{aligned} \tag{4.4}$$

For π-bonded chains, similarly at $T=0$ K, we have

$$E_{\rm tot}=\tfrac{1}{2}\gamma(\tfrac{10}{9}\Delta d_1^2)+2(\epsilon+t_0e^{-\beta\Delta d_1}) , \tag{4.5}$$

whence

$$c_\pi=\tfrac{5}{9}\gamma+t_1\beta^2,\quad f_\pi=\tfrac{1}{3}t_1\beta^3 , \tag{4.6}$$

with $t_1=t_0\exp(-\beta\Delta d_1^g)$.

We note that the cubic anharmonicity f has an opposite sign in buckling ($f_b>0$) and π-bonded chains ($f_\pi<0$). Hence, by (4.3) we expect the reconstruction magnitude ϕ to decrease with T in the buckling case, and to increase for π-bonded chains. The physical reason for this latter increase is the nonlinearity of the electronic energy gain in (4.5), due, in turn, to the exponential behavior of hopping integrals.

In conclusion, the additional energy-gap shifts expected from this mechanism are

$$\Delta E_{g,b}=\frac{C}{2a^2}(H_1^g+H_2^g)\left[\frac{3f_b}{4c_b^2}\right]k_BT$$

for buckling, and

$$\Delta E_{g,\pi}=\frac{2t_1^2}{(\frac{10}{9}\gamma\beta^{-2}+2t_1)^2}k_BT$$

for π-bonded chains. With the present values of the parameters, $C=52.8$ eV, $t=0.075$ eV, $H_1^g+H_2^g=1.65$ Å, and $H_1^g-H_2^g=0.33$ Å, one can extract an additional

temperature-induced red shift of $1.72\times10^{-5}T$ for the ionic reconstruction, e.g., $\Delta E_{g,b}=-5$ meV at $T=300$ K. Since the Franck-Condon blue shift of Fig. 6 is negligible in this case, we conclude that the weak red shift just calculated is all one expects for buckling. On the other hand, with π-bonding parameters of $t_1=-0.9$ eV, $\beta=2.7$ Å^{-1}, and $\gamma=22.3$ eV Å^{-2}, we expect an additional blue shift of $5.1\times10^{-5}T$, or $\Delta E_{g,\pi}=+15$ meV at 300 K. This amount is not sufficient to offset the large red Fan shift for this case. Table III summarizes the total changes in peak positions expected as a function of T for the two models of Si(111)2×1. The red shifts predicted for the two cases are almost 1 order of magnitude different. It seems possible that experimental investigation of this point might bring further information on the actual nature of this reconstruction, which is otherwise still uncertain, since new evidence keeps appearing which conflicting points sometimes towards π-bonded chains,[40,54,55] or towards buckling-type reconstructions,[56] or neither.[57] The room-temperature absorption spectrum of the Si(111)2×1 surface is shown on Fig. 14. Its shape seems roughly compatible, after damping is considered, with both the buckling-model result of Fig. 6 and the π-bonded chain model of Fig. 13. Its temperature dependence has not yet been studied experimentally. However, very recent polarized-light results[54] seem to yield selection rules which favor the π-bonded chain model.

It is interesting that the T-dependent absorption spectrum measured very recently on a different surface, the Si(111)7×7, shows precisely a red-shifting peak, with a shift of about 40 meV between 15 and 30 K,[58] which is very similar to the predicted π-bonded chain value of Table III for Si(111)2×1.

B. Luminescence

The emission behavior for a weak- and strong-coupling system is very different. For weak coupling, absorption and emission occur at the same frequency. For strong coupling, the emission line is Stokes-shifted by an amount $\sim 2S\hbar\omega_0$ towards the red. If one includes finite carrier lifetimes in a strong-coupling case, a two-lobed spectrum, such as that discussed by Almbladh,[59] may also be expected.

No experimental luminescence spectra of Si(111)2×1 are available to date. However, Evangelisti and McGroddy[60] have studied the closely analogous case of Ge(111)2×1 and find no surface luminescence at $\hbar\omega$ larger than 0.2 eV. If this could be simplistically taken as representative of the Si(111)2×1 as well, it would imply a Stokes shift larger than 0.3 eV. Our estimated Stokes shift in the buckling model is $\gtrsim 0.4$ eV, which would suggest exactly this outcome. Hence a careful experimental study of luminescence from Si(111)2×1 can yield crucial information on the actual existence of such a surface Stokes shift.

In the chain-model case, however, an alternative explanation for the lack of luminescence could be thermalization of electron-hole pairs created by light into *triplet* excitons (of much lower energy than the singlets) whose radiative decay is then forbidden, or very weak. Our estimate for the relaxed triplet-exciton energy for the π-bonded chain model is ~ 0.1 eV, to be compared with the value ~ 0.45 eV for the relaxed singlet exciton.

TABLE III. Position of the absorption peak as a function of temperature for the buckling and π-bonded chain models of Si(111)2×1. In both cases, the calculated values include the lattice-dilation effects and coupling to the vibrational modes.

T (K)	$\hbar\omega_{\text{peak}}$ (eV) (buckling)	$\hbar\omega_{\text{peak}}$ (eV) (π-bonded chains)
2	0.47(0)	0.49(4)
152	0.47(0)	0.49(8)
302	0.46(8)	0.46(5)
452	0.46(5)	0.42(3)
602	0.46(2)	0.38(0)

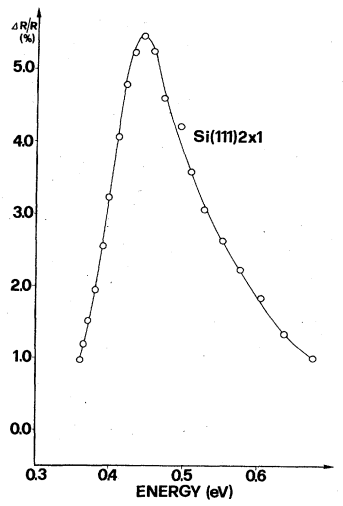

FIG. 14. Room-temperature optical absorption (as given by the change of reflectance upon oxidation) of the Si(111)2×1 surface (after Chiaradia *et al.*, Ref. 54).

C. Photoemission

Valence ultraviolet photoemission and x-ray photoemission spectroscopy (UPS and XPS) studies of surface states on Si(111) have been very numerous—if somewhat confusing[1,40,61] over the last decade. The view that a photoemission process must as a rule be assumed to be sudden from the lattice point of view justifies the complete neglect of all polaron effects—except for a broadening, of the kind discussed by Hedin and Rosengren[62] for a core line—in photoemission spectra.

There may, however, be one kind of polaron side effect that appears not to have been discussed so far. What makes a photoemission process generally a fast one is evidently *not* the high energy of excitation, but rather the short lifetimes of the end products, i.e., the electron and the hole. In particular, the hole inverse lifetime increases very fast away from the Fermi level.[20] This suggests, however, that sufficiently long hole lifetime could be achieved when photoemitting from a narrow energy shell around the Fermi level. The lifetime of a high-energy

electron, however, will be generally short, if the corresponding wavepacket crosses any amount of bulk. For example, the plasmon mean free path at $E=100$ eV is only ~ 5 Å. If we, however, consider electrons photoemitted from a surface state into a final state described by a wavepacket whose trajectory moves away from the surface without scattering further off the electrons of the sample, it might be conceivable to attain a lifetime longer than 10^{-13} sec. If this situation, admittedly rather speculative, were achieved, then in surface photoemission from a state very near E_F a hole polaron can form, and the hole-polaron shift would be transferred to the outgoing electron. Thus the high-energy part of the photoemission spectrum would not terminate at the "bare" E_F^0, but would extend above it with a tail, or an extra peak, reaching to a higher "renormalized" $E_F=E_F^0+E_{\rm pol}$. For strongly coupled polarons, such as those discussed in Sec. II, $E_{\rm pol}$ is a measurable quantity of ~ 0.4 eV. The distinguishing feature of this phenomenon should be a very weak k-vector dependence of the apparent "band" energy close to E_F, reflecting the heavy polaron masses of the strong-coupling case. Instead, the angular photoemission *intensity* would decrease as one moves away from $k=k_F$, reflecting the localized nature of the hole.

An effect of this kind may already have been observed in photoemission from the chalcogenide layer compounds.[63] It seems possible to envisage a similar explanation for the peak just below E_F seen by Himpsel *et al.*[61] on the Si(111)2×1 surface. In this interpretation of their data, the peak at -0.75 eV would constitute the bare surface-state "band." The peak at -0.15 eV would be the "polaron" peak, which is stronger at point $\bar{J}$, in agreement with the fact that the Fermi level of the bare band is closest to E_F at that point. The extracted hole-polaron shift of 0.6 eV is of the right order of magnitude for a localized hole, for which our model gave 0.4 eV.

D. Surface-state—polaron effects in scanning tunneling microscopy

The great usefulness of tunneling of electrons from a sample surface to a metal tip in the study of surface structure has been recently demonstrated experimentally.[50] The tunneling process occurs between electron states on the metal tip and the outermost surface states protruding towards the tip. If V is the voltage drop between the tip and the surface, then tunneling will occur from surface states lying within a depth V from the Fermi surface. Incidentally, this implies that this experimental technique is potentially extremely interesting when used to study spectra taken as a function of V (positive V would bring information on the filled surface states, negative V on the empty ones). To this date no such study has yet been published, although it seems possible for this technique to develop into a powerful new form of spectroscopy of the surface *electron* structure (while real-space scanning has already been shown to yield a valuable microscopy of the surface *atomic* structure).

Surface-state—polaron effects may be expected to play an interesting role in the future interpretation of the voltage surface-state spectroscopy suggested above. Let us consider, to start, the case of V positive, when an electron, originally belonging in a filled surface band, tunnels away from it to flow into the metal tip, leaving a hole behind in the surface state. Two extreme types of situations can be envisaged. If the electron stripping process is "fast," the lattice has no time to adjust and form a polaron around the hole. Then the hole energy will be uninfluenced by polaron effects, which can thus be ignored. This is the straightforward analog of a Franck-Condon transition, such as that described for optical absorption, or a photoemission process. If, on the other hand, the electron stripping occurs slowly enough, the surface lattice will have time to form a polaron about the hole, whose energy will then be shifted upwards by the amount calculated in the preceding sections.

The relevant question is then how "long" does it take for a surface electron to tunnel from the surface state into the tip? This question, as it turns out, has been rather extensively discussed in the literature, with somewhat variable conclusions. Following Leggett,[64] one may define two kinds of times in the problem. One is $\tau_0=\hbar/\Gamma$, with

$$\Gamma \sim \text{const} \times \exp[-d(2m\phi/\hbar^2)^{1/2}] ,$$

for a barrier of height ϕ and thickness d. Another is $\tau_1=d(m/2\phi)^{1/2}$. The time τ_1 is the "bounce time" over which a successful tunneling event takes place; the time τ_0 is the average time one has to wait for a successful attempt which can clearly be very much longer than τ_1. For d of a few angstroms and $\phi\sim 5$ eV, τ_1 is of the order of 10^{-15} sec. We note that this value is about 2 orders of magnitude shorter than the typical lattice readjustment time.

It is at present unclear to us whether the relevant time scale to discuss possible surface-polaron formation during tunneling is τ_0, or τ_1, and this problem will require a separate investigation. The viewpoint that all holes are the result of only successful attempts, each of which lasts the short time τ_1, would lead to the conclusion that polarons have no time to form and are irrelevant to tunneling. If, alternatively, we consider that electrons do leave the surface state anyhow, to venture, successfully or not, into the tunneling region with time scale τ_0, then a surface-state polaron may be ready around the hole if $\tau_0 > 10^{-13}$ sec, or not ready if $\tau_0 < 10^{-13}$ sec. In this case, what appears to be a rather sudden shift of hole energy should show up, in the voltage spectroscopy suggested above, as a function of surface-tip distance d, i.e., of current, which depends exponentially on d.

E. Wigner crystallization of carriers in surface states

It is well known that the surface states of semiconductors can be replenished, or emptied of electrons, by varying the bulk doping level. In particular, it is known from studies of band bending[65] that on the Si(111)2×1 surface electrons as many as $n\sim 5\times 10^{13}/\text{cm}^2$ can be driven into the upper surface-state band—or out of the lower surface-state band—by strong bulk n doping, or p doping. This is quite a large density, and it may not be totally academic to speculate about the state of these excess surface-state electrons. A mean distance of the order of

10 Å is already substantially smaller than the average distance of two surface defects on a good-quality surface, and so defects can be approximately ignored. In the absence of polaron effects, one would normally expect two-dimensional electrons of this density to be fluid at $T=0$ K. In fact, here,

$$r_s \sim (m^*/\bar{\epsilon} a_B \sqrt{\pi n}) \sim 3$$

(if $\bar{\epsilon} \sim 6$ is an effective surface screening, a_B is the Bohr radius, and a mass $m^*=1$ is assumed). The effect of strong electron-lattice coupling, however, is that of enormously increasing the effective electron mass. The hole-polaron mass for the buckling model of Sec. II, for example, was ~ 4000. An electron, or a hole, trapped inside a small polaron of this kind, is essentially a classical object. Classical two-dimensional electrons will "Wigner-crystallize," neglecting other effects due to long-range fluctuations, all the way from $T=0$ K up to a melting temperature T_M,[66] given approximately by

$$\Gamma = (k_B T_M)^{-1} (e^2/\bar{\epsilon}) \sqrt{\pi n} \sim 130 \ .$$

From this, we estimate a melting temperature as high as 25 K. Although residual quantum effects may reduce this temperature, it is nevertheless still substantially higher than two-dimensional melting temperatures seen for electrons on liquid-He surfaces,[67] of order of 0.4 K. In conclusion, we suggest that excess surface-state electrons or holes that are responsible for band bending in a doped semiconductor may be self-trapped polarons and, hence, essentially classical objects. As such, they should crystallize at sufficiently low temperature. The crystalline state might become observable experimentally. For example, deformation potentials generate a coupling mechanism between the two-dimensional plasmonlike modes of this crystal and the Rayleigh wave of the semiconductor. In a way similar to that of electrons on He,[67] this mechanism would lead to folding of the Rayleigh wave from $K=G=4\pi(n/2\sqrt{3})^{1/2} \sim 0.5$ Å^{-1} back to $k=0$. In analogy to that case, mixing with the plasmon would make this mode, of frequency as high as 15 meV, optically active and thus observable with either ir absorption or high-resolution electron-energy-loss spectroscopy.

V. CONCLUDING REMARKS

The main aim of this paper has been to introduce the concept, and show the relevance of, polaron effects on electrons that belong in surface states.

This has been pursued by direct study of prototypical situations. For this purpose, the 2×1 reconstructed Si(111) surface has been selected, as a system that has received very considerable attention in the past and for which polaron effects, not discussed before, may be of considerable importance. Among the existing models for the reconstructed surfaces, we have chosen the most popular, i.e., buckling and π-bonded chains. Polaron effects are shown to be very important in either model, and quantitatively more than an order of magnitude larger than in bulk Si, or about as important as in a three-dimensional ionic crystal.

Since strict surface-state transport will probably never be measurable, the main impact of surface-state polarons should be on the spectroscopy of surface states. We have concerned ourselves here mostly with optical absorption. A careful polaron study of the electron-hole pairs has been carried out in this light, and a detailed analysis of the absorption line shape is presented, which also brings out interesting differences between the two reconstruction models. A short discussion at a much more qualitative level is given for surface luminescence, photoemission, and scanning tunneling spectroscopy, as well as for a possible classical crystallization of a dense system of surface-state polarons. Our hope is that this paper will stimulate new experimental efforts aimed at elucidating the importance of these polaron effects in surface-state spectroscopy.

Note added in proof. In a recent paper, F. Flores, C. Tejedor, and E. Louis [Proceedings of the 17th International Conference on the Physics of Semiconductors (unpublished)] have considered a related problem of surface-state—electron-phonon coupling together with electron-electron interaction. Their results show that the presence of electron-electron interaction does add new interesting features to the problem.

ACKNOWLEDGMENTS

One of us (C.D.C.) wishes to thank Professor P. Budinich and Professor L. Fonda for a fellowship grant and for hospitality at Scuola Internazionale Superiore di Studi Avanzati.

APPENDIX A: ESTIMATE FOR THE NUMERICAL VALUES OF THE PARAMETERS C, γ, AND H_0' IN THE BUCKLING MODEL

In order to determine quantitatively the equilibrium values of H_1 and H_2 given by Eqs. (2.13), we must specify the parameters C, γ, and H_0'. For C we simply take the value $C=52.8$ eV, corresponding to $\epsilon_p - \epsilon_s = 4.4$ eV, a value introduced empirically by Pandey and Phillips[28] to fit other accurate bulk and surface-state calculations. The elastic constant γ and the reference height H_0' are, in fact, properties of a hypothetical Si(111) surface which (a) has no electrons at all in the DB state, and (b) is ideal, i.e., unreconstructed. We determine them in the following way. Suppose we start with Si(111) in this hypothetical situation, and then "pour in" the $2N$ surface electrons while keeping the surface unreconstructed. The total-energy change per atom is then

$$\mathscr{E}(H) = \tfrac{1}{2}\gamma(H - H_0')^2 + \epsilon(H) \ , \tag{A1}$$

where ϵ is the energy of one electron per DB,

$$\epsilon(H) = \epsilon_p - (C/2)(H/a)^2 \ .$$

Minimization of (A1) yields

$$H_0 = \frac{\gamma a^2 H_0'}{\gamma a^2 - C} \ . \tag{A2}$$

If we fix $H_0=0.79$ Å, the expected interlayer spacing in the absence of relaxation, then (A2) connects γ and H_0'. For a small uniform displacement Q from equilibrium,

the total energy (A1) becomes

$$\mathscr{E}(H_0+Q)=\text{const}+\tfrac{1}{2}(\gamma-C/a^2)Q^2 . \tag{A3}$$

We can relate $\gamma-C/a^2$ to the frequency ω_0 of the surface phonon characterizing the outward-inward relaxation mode of the surface by

$$\tfrac{1}{2}(\gamma-C/a^2)=\tfrac{1}{2}M\omega_0^2 , \tag{A4}$$

where M is the atomic mass. We take $\hbar\omega_0=50$ meV, a value of the order of a general short-wavelength phonon in silicon, and also close to the experimental value of the surface-phonon energy observed on Si(111)2×1.[68] This yields $\gamma a^2-C\sim250$ eV, and from (A2) we obtain $H_0'=0.65$ Å. Comparison with $H_0=0.79$ Å shows that "pouring in" one electron per DB has produced an *outward* surface relaxation. This was, of course, to be expected since outward relaxation of the first layer, by Eqs. (2.1) and (2.2), increases the s admixture in the DB wave function relative to p_z, and ϵ_s is about 4 eV lower than ϵ_p.

APPENDIX B: CALCULATION OF THE SELF-ENERGY (3.37)

For $\omega_{k'}\equiv\omega_0$ and $V_{kk'}\equiv V$ (independent of $\vec{k}$ and $\vec{k}'$), Eq. (3.37) can be rewritten in a slightly more convenient form,

$$\Sigma(E)=|V|^2(n_{\omega_0}+1)\sum_{k'}\frac{1}{E-\epsilon_{k'}-\hbar\omega_0-\Delta(E-\hbar\omega_0)-i\Gamma(E-\hbar\omega_0)}+|V|^2 n_{\omega_0}$$
$$\times\sum_{\vec{k}'}\frac{1}{E-\epsilon_{k'}+\hbar\omega_0-\Delta(E+\hbar\omega_0)-i\Gamma(E+\hbar\omega_0)} , \tag{B1}$$

where we have taken into account the independence of $\Sigma_k(E)$ on $\vec{k}$ and used $\Sigma(E)=\Delta(E)+i\Gamma(E)$. For our dimerized chain model the sums over $\vec{k}'$ reduce to one-dimensional integrals from $-\pi/a$ to π/a along the $\bar{\Gamma}\bar{J}$ direction of the SBZ. For the simple effective-mass dispersion $\epsilon_k=k^2/2m^*$, these integrals can be carried out analytically. However, before writing their expressions—which are quite cumbersome—it is convenient to establish a few notations. Separating the real and imaginary parts of $\Sigma(E)$ on the left-hand side of (B1), we can write

$$\Delta(E)=\frac{1}{2}\frac{|V|^2}{(\epsilon_L\hbar\omega_0)^{1/2}}[(1+n_{\omega_0})\Delta_1(E)+n_{\omega_0}\Delta_2(E)] , \tag{B2}$$

$$\Gamma(E)=\frac{1}{4}\frac{|V|^2}{(\epsilon_L\hbar\omega_0)^{1/2}}[(1+n_{\omega_0})\Gamma_1(E)+n_{\omega_0}\Gamma_2(E)] , \tag{B3}$$

where $\epsilon_L=\hbar^2\pi^2/2m^*a^2$. Let us next define ($i=1,2$)

$$\varphi_i(E)=\arg A_i(E) , \tag{B4}$$

$$Q_i(E)=|A_i(E)|^{-1} , \tag{B5}$$

$$R_i(E)=\text{Re}[A_i^{-1}(E)] , \tag{B6}$$

$$I_i(E)=-\text{Im}[A_i^{-1}(E)] , \tag{B7}$$

where

$$A_1(E)=\frac{1}{E-\hbar\omega_0-\Delta(E-\hbar\omega_0)-i\Gamma(E-\hbar\omega_0)} \tag{B8}$$

and

$$A_2(E)=\frac{1}{E+\hbar\omega_0-\Delta(E+\hbar\omega_0)-i\Gamma(E+\hbar\omega_0)} . \tag{B9}$$

We start with $\Gamma_i(E)$, which has a somewhat simpler expression,

$$\Gamma_i(E)=\left[\frac{\hbar\omega_0}{Q_i}\right]^{1/2}\left[\sin(\varphi_i/2)\ln\left|\frac{\epsilon_L+2(\epsilon_L Q_i)^{1/2}\cos(\varphi_i/2)+Q_i}{\epsilon_L-2(\epsilon_L Q_i)^{1/2}\cos(\varphi_i/2)+Q_i}\right|+2\cos(\varphi_i/2)(\theta_i+\pi/2)\right] , \tag{B10}$$

with

$$\theta_i(E)=\tan^{-1}\frac{\epsilon_L-Q_i}{2(\epsilon_L Q_i)^{1/2}\sin(\varphi_i/2)} . \tag{B11}$$

For the two terms contributing to $\Delta(E)$ in (B2), we find

$$\Delta_i(E)=\left[\frac{\hbar\omega_0}{Q_i}\right]^{1/2}\left[\frac{R_i+Q_i}{2I_i}\sin(\varphi_i/2)\ln\left|\frac{\epsilon_L+2(\epsilon_L Q_i)^{1/2}\cos(\varphi_i/2)+Q_i}{\epsilon_L-2(\epsilon_L Q_i)^{1/2}\cos(\varphi_i/2)+Q_i}\right|+\frac{\cos(\varphi_i/2)}{\sin\varphi_i}\left[\frac{R_i}{Q_i}(\theta_i+\pi/2)-\theta_i^+-\theta_i^-\right]\right] , \tag{B12}$$

where

$$\theta_i^{\pm}(E)=\tan^{-1}\frac{(\epsilon_L)^{1/2}\pm(Q_i)^{1/2}\cos(\varphi_i/2)}{(Q_i)^{1/2}\sin(\varphi_i/2)} . \tag{B13}$$

We recall that all terms, such as Q_i, R_i, φ_i, etc. in (B10) and (B12) are functions of E through (B4)—(B7).

The expressions (B2) and (B3)—with (B10) and (B12)—are already in a form which can be easily programmed for a numerical iterative solution, starting, for instance, from $\Delta(E)\equiv 0$ and $\Gamma(E)\equiv\gamma\ll 1$ (a small but finite value of γ is, of course, necessary to avoid divergencies). To test the convergence we monitored the value $\mathcal{I}$ of the integral of the spectral function,

$$\mathcal{I}=\frac{1}{\pi}\int dE\frac{\Gamma(E)}{[E-\Delta(E)]^2+\Gamma^2(E)} .$$

Good convergence ($<10^{-4}$) usually requires about 20 iterations.

[1]For a review of UPS up to 1980, see D. E. Eastman, J. Vac. Sci. Technol. **17**, 492 (1980).

[2]G. Chiarotti, S. Nannarone, R. Pastore, and P. Chiaradia, Phys. Rev. B **4**, 3398 (1971); P. Chiaradia, G. Chiarotti, S. Nannarone, and P. Sassaroli, Solid State Commun. **26**, 813 (1978).

[3]J. E. Rowe and H. Ibach, Phys. Rev. Lett. **31**, 102 (1973); R. Matz, H. Lüth, and A. Ritz, Solid State Commun. **46**, 343 (1983).

[4]M. Schlüter, J. R. Chelikowsky, S. G. Louie, and M. L. Cohen, Phys. Rev. B **12**, 4200 (1975).

[5]J. A. Appelbaum and D. R. Hamann, Rev. Mod. Phys. **48**, 479 (1976).

[6]J. E. Northrup, J. Ihm, and M. L. Cohen, Phys. Rev. Lett. **47**, 1910 (1981).

[7]K. C. Pandey, Phys. Rev. Lett. **49**, 223 (1982).

[8]J. E. Northrup and M. L. Cohen, Phys. Rev. Lett. **49**, 1349 (1982).

[9]E. Tosatti, in *Festkörperprobleme (Advances in Solid State Physics)* edited by H. J. Queisser (Pergamon/Vieweg, Braunschweig, 1975), Vol. XV, p. 113.

[10]K. Thoma, Z. Phys. B **23**, 49 (1976).

[11]G. Allan and M. Lannoo, Surf. Sci. **63**, 11 (1977).

[12]C. T. White and K. L. Ngai, Phys. Rev. Lett. **41**, 885 (1978).

[13]R. Del Sole and D. J. Chadi, Phys. Rev. B **24**, 1120 (1981).

[14]C. B. Duke and W. K. Ford, Surf. Sci. **111**, L685 (1981).

[15]A. Muramatsu and W. Hanke, Phys. Rev. B **27**, 2609 (1983).

[16]A. Muramatsu and W. Hanke, in *Ab initio Calculation of Phonon Spectra,* edited by J. T. Devreese, V. E. Van Doren, and P. E. Van Camp (Plenum, New York, 1983).

[17]F. Guinea and C. Menéndez, Phys. Rev. B **27**, 1432 (1983).

[18]D. Haneman, Phys. Rev. **121**, 1093 (1961).

[19]K. C. Pandey, Phys. Rev. Lett. **47**, 1913 (1981).

[20]J. J. Quinn and R. A. Ferrell, Phys. Rev. **112**, 812 (1958).

[21]F. Bassani and G. Pastori Parravicini, *Electronic States and Optical Transitions in Solids* (Pergamon, New York, 1975).

[22]R. Del Sole and E. Tosatti, Solid State Commun. **22**, 307 (1977).

[23]H. Haken, in *Polarons and Excitons,* edited by C. G. Kuper and G. D. Whitfield (Oliver and Boyd, Edinburgh, 1962).

[24]S. D. Mahanti and C. M. Varma, Phys. Rev. B **6**, 2209 (1972).

[25]M. Rovere and E. Tosatti, Nuovo Cimento **39B**, 538 (1977).

[26]Y. Toyozawa, in *The Physics of Elementary Excitations,* Vol. 12 of *Springer Series in Solid State Sciences,* edited by S. Nakajima, Y. Toyozawa, and R. Abe (Springer, Berlin, 1980), Chap. 7.

[27]G. Chiarotti, in *Theory of Imperfect Crystalline Solids, Trieste Lectures, 1970* (IAEA, Vienna, 1971).

[28]K. C. Pandey and J. C. Phillips, Phys. Rev. Lett. **32**, 1433 (1974); **34**, 1450 (1975); Phys. Rev. B **13**, 750 (1976).

[29]H. Fröhlich, in *Polarons and Excitons,* Ref. 23.

[30]W. Andreoni and E. Tosatti, in *Proceedings of the 7th International Vacuum Congress and 3rd International Conference on Solid Surfaces, Vienna, 1977,* edited by R. Dobrozemski, F. Rüdenauer, F. P. Viehböck, and A. Breth (Berger, Vienna, 1977), p. 591.

[31]It should be noted, however, that the ionic charge transfer would not be quite so large had intra-atomic electron-electron repulsions been considered. This is an artifact of the one-electron Hamiltonian (2.3), which for the present purposes does not have any negative consequence.

[32]As a general reference, see, e.g., *Polarons and Excitons,* Ref. 23.

[33]This decay is actually exponential, at least in a simple model such as ours, where all vibrational frequencies are finite (Einstein-like).

[34]This balance is qualitatively very similar to that of a Jahn-Teller distortion h, where the total energy has a form $E=-\alpha h$(electronic)$+\beta h^2$(lattice). In this case, exactly half of the electronic gain is absorbed by the lattice distortion.

[35]See, e.g., W. Kohn, in *Lectures in Theoretical Physics,* edited by C. De Witt and R. Balian (Gordon and Breach, New York, 1967).

[36]E. Clementi and C. Roetti, At. Data Nucl. Data Tables **14**, 177 (1974).

[37]M. Schlüter, in Proceedings of the International School of Physics "Enrico Fermi," Varenna, edited by F. Bassani, F. Fumi, and M. Tosi (unpublished).

[38]K. C. Pandey, Phys. Rev. B **25**, 4338 (1982). Recent measurements of the surface reflectivity of Si(111)2×1 using polarized radiation seem to actually favor a symmetric (probably somewhat buckled) chain configuration rather than the dimerized (asymmetric) one discussed in this paper (see Ref. 54). Polaron effects, however, are expected to be qualitatively similar for the two cases. In particular, the buckled chain is also an intermediate-coupling situation.

[39]W. P. Su, J. R. Schrieffer, and A. J. Heeger, Phys. Rev. B **22**, 2099 (1980); **28**, 1138(E) (1983).

[40]R. I. G. Uhrberg, G. V. Hansson, J. M. Nicholls, and S. A. Flodström, Phys. Rev. Lett. **48**, 1032 (1982).

[41]Actually, the strong analogy with polyacetylene raises the question of whether solitons could occur on this π-bonded chain model (Ref. 39). We have chosen not to pursue the issue of solitons in this paper. Should the π-bonded dimerized

chain model be definitely established for Si(111)2×1 surface, this issue might well be worth taking up again.

[42]This fact follows generally for any situation where the energy change is of the form $\Delta E=\alpha_1 d+\alpha_2 d-\frac{1}{2}\gamma d^2$, where $\langle \Delta E \rangle_{\min}=2\alpha^2/\gamma+2\alpha^2/\gamma-2\alpha^2/\gamma$ if $\alpha_1=\alpha_2\equiv\alpha$. Hence, exact cancellation between the filled-band contribution and the elastic term is expected to occur, for example, also in the case of polyacetylene, which has a similar band structure.

[43]T. Holstein, Ann. Phys. (N.Y.) **8**, 325 (1959).

[44]L. Hedin and S. Lunqvist, in *Solid State Physics,* edited by F. Seitz, D. Turnbull, and H. Ehrenreich (Academic, New York, 1969), Vol. 23, p. 1.

[45]C. Kittel, *Quantum Theory of Solids* (Wiley, New York, 1963).

[46]T. Ando, A. Fowler, and F. Stern, Rev. Mod. Phys. **54**, 437 (1982).

[47]L. V. Keldysh, Pis'ma Zh. Eksp. Teor. Fiz. **29**, 716 (1979) [JETP Lett. **29**, 658 (1979)].

[48]R. Del Sole and A. Selloni, Phys. Rev. B **30**, 883 (1984).

[49]In this respect, it is interesting to note that the resulting "triplet exciton condensate" would be an insulator with negligible dimerization, in strong analogy to the state suggested by A. A. Ovchinnikov, I. I. Ukrainskii, and G. V. Kventsel, Usp. Fiz. Nauk. **108**, 81 (1972) [Sov. Phys.—Usp. **15**, 575 (1973)] for polyacetylene and other one-dimensional chain systems. It is not clear to us whether the question of triplet excitons has been investigated at all in polyacetylene.

[50]G. Binnig, H. Rohrer, Ch. Gerber, and E. Weibel, Phys. Rev. Lett. **49**, 57 (1982); **50**, 120 (1983).

[51]H. Y. Fan, Phys. Rev. **82**, 900 (1951).

[52]V. Heine and J. A. Van Vechten, Phys. Rev. B **13**, 1622 (1976).

[53]C. Kittel, *Introduction to Solid State Physics* (Wiley, New York, 1976), Chap. 6.

[54]P. Chiaradia, A. Cricenti, S. Selci, and G. Chiarotti, Phys. Rev. Lett. **52**, 1145 (1984); R. Del Sole and A. Selloni, Solid State Commun. **50**, 825 (1984).

[55]R. M. Tromp, L. Smit, and F. J. van der Veen, Phys. Rev. Lett. **51**, 1672 (1983).

[56]R. Feder, Solid State Commun. **45**, 51 (1983).

[57]H. Lui, M. R. Cook, F. Jona, and P. M. Marcus, Phys. Rev. B **28**, 6137 (1983).

[58]J. E. Demuth, B. N. J. Persson, and A. J. Schell-Sorokin, Phys. Rev. Lett. **51**, 2214 (1983).

[59]C. O. Almbladh, Phys. Rev. B **16**, 4343 (1977).

[60]F. Evangelisti and J. McGroddy, Solid State Commun. **25**, 1157 (1978).

[61]F. J. Himpsel, P. Heimann, and D. E. Eastman, Phys. Rev. B **24**, 2003 (1981); F. Houzay, G. Guichar, R. Pinchaux, G. Jezequel, F. Solal, A. Barski, P. Steiner, and Y. Petroff, Surf. Sci. **132**, 40 (1983).

[62]L. Hedin and A. Rosengren, J. Phys. F **7**, 1339 (1977).

[63]G. Sawatzky (private communication); D. K. G. de Boer, Ph.D. thesis, University of Gröningen, 1983.

[64]A. J. Leggett, Prog. Theor. Phys. Suppl. **69**, 80 (1980); see also the later discussion of M. Büttiker and R. Landauer, Phys. Rev. Lett. **49**, 1739 (1982).

[65]F. G. Allen and G. W. Gobeli, J. Appl. Phys. **35**, 597 (1964).

[66]R. C. Gann, S. Chakravarty, and G. V. Chester, Phys. Rev. B **20**, 326 (1979).

[67]C. C. Grimes and G. Adams, Phys. Rev. Lett. **42**, 795 (1979).

[68]H. Ibach, Phys. Rev. Lett. **27**, 253 (1971).